Assignment of Heme Resonances and Determination of the Electronic Structures of High- and Low-Spin Nitrophorin 2 by 1 H and 13 C NMR Spectroscopy: An Explanation of the Order of He...

ARTICLE *in* BIOCHEMISTRY · JANUARY 2003

Impact Factor: 3.02 · DOI: 10.1021/bi026765w · Source: PubMed

3 AUTHORS, INCLUDING:

F(rances) Ann Walker
The University of Arizona
242 PUBLICATIONS **9,001** CITATIONS

SEE PROFILE

Assignment of Heme Resonances and Determination of the Electronic Structures of High- and Low-Spin Nitrophorin 2 by ^{1}H and ^{13}C NMR Spectroscopy: An Explanation of the Order of Heme Methyl Resonances in High-Spin Ferriheme Proteins†

Tatjana Kh. Shokhireva, Nikolai V. Shokhirev, and F. Ann Walker*

Department of Chemistry, University of Arizona, Tucson, Arizona 85721-0041

Received August 30, 2002; Revised Manuscript Received November 15, 2002

ABSTRACT: The ^{1}H NMR resonances of the heme substituents of the low-spin Fe(III) form of nitrophorin 2, as its complexes with *N*-methylimidazole (NP2−NMeIm) and imidazole (NP2−ImH), have been assigned by a combination of ^{1}H homonuclear two-dimensional NMR techniques and $^{1}H-^{13}C$ HMQC. Complete assignment of the proton and partial assignment of the ^{13}C resonances of the heme of these complexes has been achieved. Due to favorable rates of ligand exchange, it was also possible to assign part of the ^{1}H resonances of the high-spin heme via saturation transfer between high- and low-spin protein forms in a partially liganded NP2−NMeIm sample; additional resonances (vinyl and propionate) were assigned by NOESY techniques. The order of heme methyl resonances in the high-spin form of the protein over the temperature range of 10−37 °C is 8 = 5 > 1 > 3; the NMeIm complex has 5 > 1 > 3 > 8 as the order of heme methyl resonances at <30 °C, while above that temperature, the order is 5 > 3 > 1 > 8, due to crossover of the closely spaced 3- and 1-methyl resonances of the low-spin complex at higher temperatures. This crossover defines the nodal plane of the heme orbital used for spin delocalization as being oriented 162 ± 2° clockwise from the heme $N_{II}-Fe-N_{IV}$ axis for the heme in the B orientation. For the NP2−ImH complex, the order of heme methyl resonances is 3 > 5 > 1 > 8, which defines the orientation of the nodal plane of the heme orbital used for spin delocalization as being oriented ∼150−155° clockwise from the heme $N_{II}-Fe-N_{IV}$ axis. In both low-spin complexes, the results are most consistent with the exogenous planar ligand controlling the orientation of the nodal plane of the heme orbital. In the high-spin form of NP2, the proximal histidine plane is shown to be oriented 135° clockwise from the heme $N_{II}-Fe-N_{IV}$ axis, again for the B heme orientation. A correlation between the order of heme methyl resonances in the high-spin form of NP2 and several other ferriheme proteins and an apparent 90° shift in the nodal plane of the orbital involved in spin delocalization from that expected on the basis of the orientation of the axial histidine imidazole nodal plane have been explained in terms of bonding interactions between Fe(III), the axial histidine imidazole nitrogen, and the porphyrin π^* orbitals of the high-spin protein.

The nitrophorins (nitro being NO and phorin the carrier) are NO-carrying heme proteins found in the saliva of at least two species of blood-sucking insects, *Rhodnius prolixus*, the "kissing bug", which has four such proteins (*1*), and *Cimex lectularius*, the bedbug, which has one (*2*). These interesting heme proteins sequester nitric oxide that is produced by a nitric oxide synthase (NOS)[1] enzyme that is similar to vertebrate constitutive NOS, and is present in the cells of the salivary glands (*3*−*5*), thus keeping it stable for long periods of time by binding it as an axial ligand to a ferriheme center (*6*). In the notation of Feltham and Enemark, this is a $\{FeNO\}^6$ center (*7*). Upon injection into the tissues of the victim, NO dissociates and diffuses through the tissues to the nearby capillaries to cause vasodilation and thereby allow more blood to be transported to the site of the wound. At the same time, histamine, the role of which is to cause swelling, itching, and the beginning of the immune response, is released by mast cells and platelets of the victim. In the case of the *Rhodnius* proteins, this histamine binds to the heme sites of the nitrophorins, hence preventing the insect's detection for a period of time (*8*). These two properties of

† This work was supported by National Institutes of Health Grants HL54826 and DK31038.

* To whom correspondence should be addressed: Department of Chemistry, University of Arizona, Tucson, AZ 85721-0041. Telephone: (520) 621-8645. Fax: (520) 626-9300. E-mail: awalker@u.arizona.edu.

[1] Abbreviations: NP, nitrophorin (a NO-carrying protein); NO, nitric oxide; ImH, imidazole; NMeIm, *N*-methylimidazole; NOS, nitric oxide synthase; NMR, nuclear magnetic resonance; 1D, one-dimensional; 2D, two-dimensional; NOE, nuclear Overhauser effect; NOESY, nuclear Overhauser and exchange spectroscopy; HMQC, heteronuclear multiple-quantum coherence (a 2D NMR experiment that correlates scalar coupled ^{1}H and ^{13}C signals); WEFT, water-eliminated Fourier transform (a method for suppressing signals from protons having long relaxation times); DQF-COSY, double-quantum-filtered correlation spectroscopy; TOCSY, total correlation spectroscopy; EPR, electron paramagnetic resonance; high-spin or HS, maximum number of unpaired d electrons; low-spin or LS, minimum number of unpaired d electrons; 4IPzH, 4-iodopyrazole; DMSO, dimethyl sulfoxide; THF, tetrahydrofuran.

10.1021/bi026765w CCC: $25.00
Published on Web 12/24/2002

Scheme 1

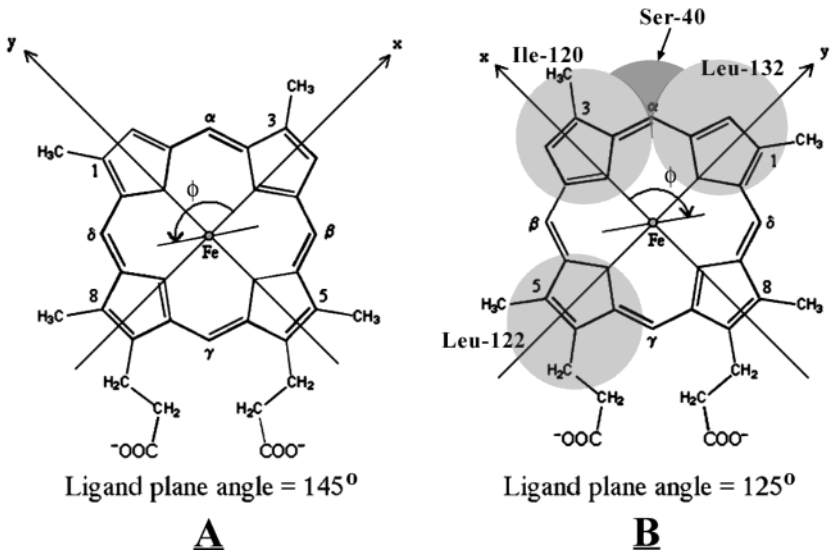

the nitrophorins of *R. prolixus* contribute to the transmission of the protozoan *Trypanasoma cruzi*, the vector of Chagas' disease (*9*), to the victim, via the feces of the insect, left behind at the site of the bite (*1*).

The *Rhodnius* proteins, which have been named NP1−4 in order of their abundances in the insect saliva, have been investigated by a number of spectroscopic techniques (*1*, *10*, *11*), spectroelectrochemistry (*1*, *11*, *12*), and stopped-flow kinetics (*12*, *13*), and the solid state structures of one or more ligand complexes of NP1 (*11*, *14*), NP2 (*15*), and NP4 (*16*−*18*) have been determined by X-ray crystallography. The structures are unique for heme proteins, in that the heme is located at the open end of a β-barrel (*19*), rather than in the more commonly observed largely α-helical globin or four-helix bundle folds. Another unusual heme protein fold, which is roughly a "hybrid" of the β-barrel and globin folds, called a PAS domain, is that of the oxygen-sensing protein FixL from the nitrogen-fixing bacterium *Bradyrhizobium japonicum* (*20*, *21*). In the *Rhodnius* nitrophorins, the ferriheme molecule is bound to the protein via a histidine ligand, leaving the sixth coordination site available to bind NO or other ligands. In the NO-off form, either water or ammonia, depending on buffer type, is bound to the sixth site in the crystals (*14*, *16*).

Of the four *Rhodnius* nitrophorins, NP2 is especially important in that, in addition to its NO releasing and histamine binding roles, it is the only one of the four proteins which has anticoagulant activity. NP2 acts in this role by inhibiting the intrinsic factor Xase complex, and its activity is independent of the presence of heme (*22*). Zhang et al. showed NP2 to be a hyperbolic mixed-type inhibitor that inhibits factor IXa-catalyzed cleavage of factor X in the presence of factor VIIIa, phospholipid, or both (*23*). Study of the detailed interaction of NP2 with factors IX and IXa suggests that NP2 interacts with a specific conformation of factor IXa found in the factor Xase complex (*23*).

One of the most important spectroscopic techniques for characterizing heme proteins is ^{1}H NMR spectroscopy. In the case of the nitrophorins, NO bound to the Fe(III) heme center produces {FeNO}^{6} diamagnetic complexes at all temperatures. In this state, all heme substituent resonances are buried in the protein proton resonance envelope, while the NO-free forms of the nitrophorins are high-spin ($S = {}^5/_2$) complexes. Binding of even-electron strong-field donor ligands, such as histamine, imidazoles, pyrazoles, or cyanide, to the NO-free forms of these proteins produces low-spin ($S = {}^1/_2$) Fe(III) complexes. The unpaired electrons on the metal of both $S = {}^5/_2$ and $S = {}^1/_2$ Fe(III) proteins act as "beacons" that "illuminate" the protons in the vicinity of the metal, by causing shifts (isotropic shifts) of the resonances from those observed in a diamagnetic protein. These shifts allow much to be learned about the intimate details of the electron configuration at the iron center. The two contributions to the isotropic shifts are the contact (through bonds) and dipolar or pseudocontact (through space) contributions; these are discussed in considerable detail elsewhere (*24*, *25*).

The proton resonances of the ferriheme center and nearby protein residues in the two paramagnetic forms of the four nitrophorins from *R. prolixus* are being investigated in detail in our laboratory. Early in this investigation, it was found that of the four similarly structured proteins, NP2 provides by far the simplest NMR spectra because (1) unlike the other three nitrophorins, NP2 exhibits only one heme orientation in the solid state (*15*) in which, if one looks down at the heme from the open sixth coordination site, with the His-57 imidazole ligand below the heme, the orientation is that known as B, i.e., where the heme substituents are arranged in a counterclockwise order in terms of increasing number, 1−8, of the β-pyrrole substituents (Scheme 1, orientation B), and (2) there are no chemical exchange cross-peaks observed in the NOESY spectra of this protein, unlike those of NP1 and NP4 (*26*, *27*).

In this work, we report the assignment of the heme resonances of NP2 in its low-spin ($S = {}^1/_2$) *N*-methylimidazole (NMeIm) and imidazole (ImH) complexes, as well as assignment of the heme resonances (except for the *meso*-H resonances and one each of the β-CH resonances of the 6- and 7-propionate groups) of this protein in its high-spin ($S = {}^5/_2$) form. Assignment of the heme resonances in both of these forms of the protein is made possible by the sharpness of the signals of the low-spin complexes, which allow NOE cross-peaks to be detected for all heme substituents, and by

a favorable rate of exchange of NMeIm between individual NP2 molecules, which allowed one-dimensional (1D) saturation transfer difference experiments to connect the methyl resonances of the high-spin complex with those of the low-spin complex which had already been assigned. NOESY spectra then allowed assignment of the vinyl and propionate resonances of the high-spin protein. In addition to the assignment of the majority of the heme proton resonances of the high-spin form of NP2, an explanation of the order of heme methyl resonances in this and a number of other high-spin ferriheme proteins, based upon the orientation of the axial histidine imidazole plane, is proposed.

EXPERIMENTAL PROCEDURES

Sample Preparation. NP2 was prepared as described previously (*11*, *13*−*15*) and stored in lyophilized form at −80 °C until it was used. NMR samples consisted of 3−6 mM solutions of the protein in D_2O containing 30 mM phosphate buffer at pH 7.0 (uncorrected for the deuterium isotope effect). To obtain the low-spin complexes, the high-spin NP2 protein was titrated with *N*-methylimidazole or imidazole until the proton NMR signals in the 70−19 ppm region disappeared. Concomitantly, these signals were replaced with signals in the 29−10 ppm region. The sample used for saturation transfer studies at 37 °C was prepared by titrating in NMeIm until the signals in the 16−10 ppm region had sufficient intensity to be clearly observed, while the majority of the sample still exhibited the high-spin Fe(III) peaks. The percent of low-spin complex in this sample was in the range of 20−30%.

NMR Data Collection. Data were collected over the temperature range of 10−37 °C with the chemical shift referenced to residual water. Temperatures higher than 37 °C were not investigated because they were not required for saturation transfer or NOESY experiments utilized for investigating chemical exchange; thus, the high-temperature limit on the stability of NP2 has not been determined. NOESY, TOCSY, HMQC, and 1D saturation transfer difference spectra were obtained on a Bruker DRX-500 spectrometer operating at a proton Larmor frequency of 500.03 MHz. The $^1H-^{13}C$ HMQC spectra were recorded using the 5 mm inverse-detection probe with decoupling during acquisition. A recycle time of 200 ms and a refocusing time of 2.5 ms (*28*) were used. The WEFT-NOESY experiment utilized a relaxation delay of 160 ms and a recovery delay of 160 ms. The mixing time for the NOESY experiments was 5−30 ms. DQF-COSY spectra were acquired using a Varian Unity-300 spectrometer operating at a proton Larmor frequency of 299.96 MHz. All 2D spectra were collected with 1024 or 2048 data points in the t_2 dimension and 256−512 blocks in the t_1 dimension with 400−800 scans/block.

RESULTS AND DISCUSSION

The ligand-free form of recombinant NP2 at pH 7.0 and 30 °C has resolved heme and hyperfine-shifted protein resonances that extend from 70 to nearly −14 ppm, as shown in Figure 1A. These heme resonances are well-resolved, with unique signals of intensities corresponding to one or three protons (except for three small peaks at 69, 68, and 56 ppm due to three of the heme methyls of ∼8−10% of the A heme

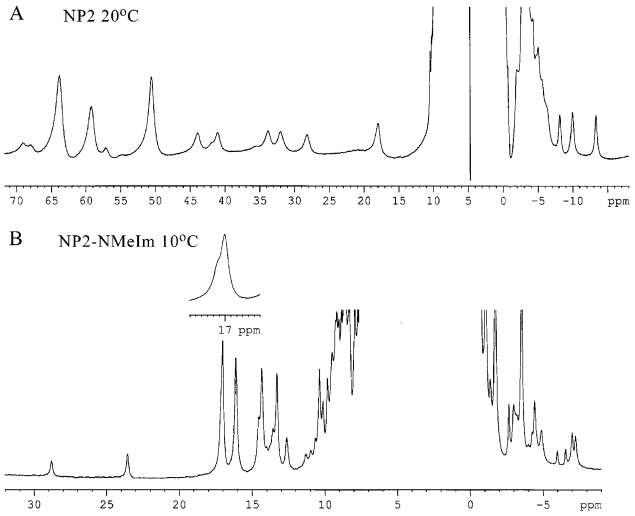

FIGURE 1: 1D ^1H NMR spectra of high-spin (A) and low-spin NMeIm complex (B) forms of NP2, recorded at 500 MHz, pH 7.0, and the listed temperatures. In panel B, the peak at 29 ppm remains unassigned at this time.

orientational isomer, Scheme 1) that are similar in general appearance to those of previously studied high-spin Fe(III) proteins, including those of metmyoglobins (*25*, *29*, *30*), cytochrome *c*′ (*31*−*33*), and the resting state of horseradish peroxidases (*34*, *35*). The ^1H NMR spectrum of high-spin NP2 is especially similar to those of elephant metmyoglobin species B (*29*), cytochrome *c*′ (*32*, *33*), and horseradish peroxidase (*34*, *35*), except that the order of heme methyl resonances is different in each of these cases, as will be discussed in detail below. The high-spin ferriheme iron in NP2 is clearly bound to His-57 [numbering system based on the deletion of two residues early in the protein sequence for NP2 and NP3, as compared to NP1 and NP4 (*1*)], and thus, different contact and dipolar shifts are experienced for different heme methyl groups and other substituents due to the orientation of the proximal histidine. No evidence of broad signals due to the *meso*-H resonances could be found in the −20 to −60 ppm region of the spectrum (not shown), which is consistent with water being bound to the sixth coordination site of the heme iron (*30*) [five-coordinate high-spin ferrihemes have *meso*-H resonances at −40 to −50 ppm, while six-coordinate high-spin ferrihemes have these resonances at ∼40 ppm (*24*, *30*)]. That water is bound to the ferriheme iron center of the high-spin nitrophorins in aqueous solution at neutral pH is also consistent with the fact that cyclic voltammetric investigation of the nitrophorins showed that they give rise to irreversible waves (*36*), which in the case of myoglobin was attributed to the loss of the axial water upon heme reduction which could not be recoordinated upon reoxidation during the time scale of the cyclic scan (*37*). A water or NH_3 molecule, depending on the buffer and/or pH, is also bound to the Fe(III) of the nitrophorins in the crystalline state (*14*−*17*).

Addition of a strong-field ligand such as *N*-methylimidazole (NMeIm) to this high-spin Fe(III) center creates the low-spin Fe(III) state, which is characterized by a range of NMR shifts much smaller and resonances much sharper than those of the high-spin form, as shown in Figure 1B. These sharper resonances are typical of all of the nitrophorins, although the pattern of heme methyl resonances differs somewhat from

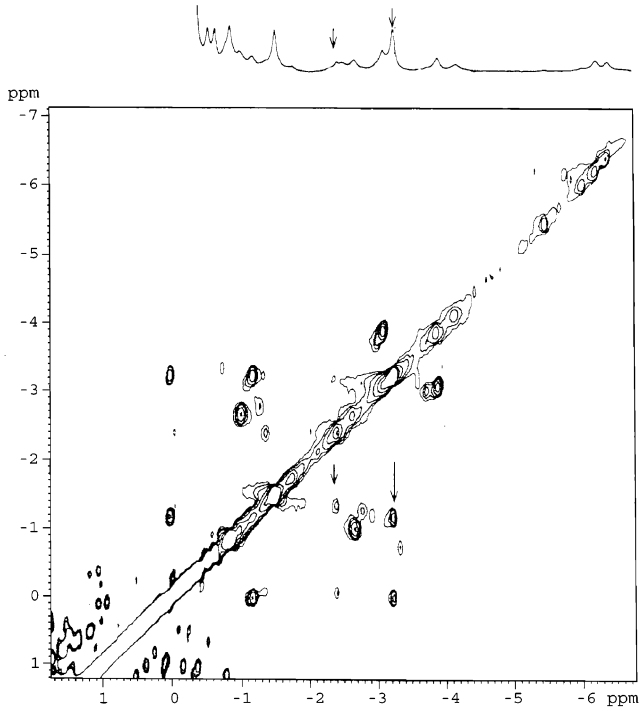

FIGURE 2: TOCSY map and 1D projection of the upfield region of the ^{1}H NMR spectrum of the NP2−NMeIm complex at 30 °C and 500 MHz, showing the coupling patterns of two isomers.

protein to protein, as will be discussed in detail elsewhere (*26*). On the basis of the pattern of observed heme substituent resonances (*38*), the heme in solution has the B orientation (Scheme 1), as seen in the solid state (*15*). However, addition of NMeIm creates two similar patterns of resonances for Ile-120 with very similar chemical shifts that have very different intensities in the TOCSY map obtained at 30 °C, as shown in Figure 2, as well as in the DQF-COSY and WEFT-NOESY maps discussed below. (Ile-120 is located in the distal pocket, between Leu-122 and Leu-132; it is above pyrrole ring II, as shown in Scheme 1, orientation B, and is expected to interact with the methyl group of NMeIm in one, but not the other, of its possible "seatings" that maintains the same ligand plane orientation.) The ratio of the two species is ∼3:1. Doubling of the *N*-methyl resonance of the coordinated ligand, as shown in the inset of Figure 1B, is also observed and also results from the two possible locations of the *N*-methyl group that result from the two seatings of this unsymmetrical ligand, as will be discussed below in reference to the WEFT-NOESY spectrum.

In addition to this doubling of Ile-120 and *N*-methyl ligand resonances, there are also two sets of heme propionate resonances for both 6- and 7-propionates, as well as the γ-*meso*-H and the 5Me group. No chemical exchange is observed between these sets of major and minor resonances at 10 °C or at any higher temperatures that have been investigated (up to 37 °C; temperatures higher than this were not needed for the chemical exchange investigations discussed below, and hence were not investigated). Protein dynamics on a time scale too slow for detection by NMR spectroscopy could also be a source of the different isomers that have been observed; such protein motions could be either global, such as movement of the loop between the A and B and that between the G and H β-sheets of the protein, the conformation of which is known to change upon binding of NO or imidazole (*17*, *18*), or more local, and in either case create two different patterns of propionate proton resonances, which are observed for both low-spin complexes, NP2−NMeIm and NP2−ImH. The A−B and G−H loops are near the distal side of the heme, and in the case of NP4, their positions change significantly upon loop closure (*17*, *18*); no closed loop structure of NP2 is yet available for comparison. In contrast, the protein side chain closest to the 6- and 7-propionate part of the heme on the proximal (His-57) side is the phenyl ring of Phe-66, which is parallel to and within π contact (closest distance of 3.4 Å) with the His-57 imidazole ring; the two *meta* carbons of the phenyl ring are within 3.7−4.0 Å of the 6- and 7-β-carbons of the propionate group, and the *para* carbon is within 3.75 Å of the γ-*meso* carbon (*15*). There is only one conformation for Phe-66 in the crystal structure (*15*), but it could be that there are two conformations present in solution, which interconvert too slowly at 10 °C for chemical exchange between them to be detected. A similar type of doubling of the propionate resonances is observed for the NP2−ImH imidazole complex [Supporting Information, Figure S1b]. No crystal structure of the NP2−NMeIm or NP2−ImH complex is currently available to allow assessment of potential changes in the Phe-66 side chain or A−B and G−H loop conformations, so at present, it is not possible to determine the reason for the two sets of resonances observed in the 1D, TOCSY, DQF-COSY, and NOESY spectra.

The existence of multiple species in the same NMR sample led us, on one hand, to utilize lower temperatures for NOESY experiments to maximize the intensity of NOE cross-peaks and minimize any chemical exchange that might occur at higher temperatures and, on the other hand, to use higher temperatures to obtain sharper and more intense paramagnetically shifted peaks, especially for the ligand-free high-spin protein. As a result, we present, in the tabulated data (Tables 1 and 2, for the *N*-methylimidazole and imidazole complexes, respectively) and figures, results obtained at different temperatures (with the temperature always given). Thus, the protons of the heme that are investigated in this work using different 1D and 2D NMR techniques show differences in chemical shift with temperature, due to the temperature dependence of the chemical shifts of these paramagnetic systems. Figure 3 shows the Curie plot for the heme methyl resonances of the NMeIm complex; note that the order of 1Me and 3Me reverses above ∼30 °C. Table 1 includes the chemical shifts of the assigned proton signals at four temperatures.

Identification and Assignment of the Four Heme Methyl Resonances for the NP2−NMeIm and NP2−ImH Complexes. In Figure 1B, four methyl resonances of the NP2−NMeIm complex that are shifted from the diamagnetic region into the downfield region outside the envelope of protein resonances are observed at 16.9 (actually two resonances, at 17.0 and 16.9 ppm), 15.9, 14.2, and 13.2 ppm at 10 °C. There are four carbon resonances at 25.8, −32.9, −24.3, and −36.3 ppm, corresponding to these four proton resonances, respectively, in the HMQC map at 20 °C, shown in Figure 4. The first of these, at 16.4 (^{1}H) and 25.8 ppm (^{13}C) in Figure 4 [mentioned above for the 10 °C 1D ^{1}H spectrum of Figure 1B (inset) where the ^{1}H resonances occur at 16.9 and 17.0 ppm], is easily shown to be the *N*-methyl group of NMeIm

Table 1: NP2−NMeIm ^{1}H and ^{13}C Heme Assignments in D_2O at pH 7.0 at Four Temperatures

	^{1}H resonance (ppm)				^{13}C resonance (ppm)
substituent	10 °C	20 °C	25 °C	30 °C	20 °C
N-methyl	16.9 (17.0)[a]	16.4 (16.5)[a]	16.1		25.8
5Me	15.9 (15.8)[a]	15.6	15.4		−32.9
1Me	14.2	13.9	13.8		−24.3
3Me	13.2	13.3	13.4		−36.3
8Me	−0.2	0.6	1.0		−4.6
6P H_α	14.6 (14.0)[a,b]	14.0	13.9	13.8	−45.5
6P $H_{\alpha'}$	12.6 (11.2)[a,b]	12.6	12.5	12.3	−45.5
6P H_β	−1.3 (−1.5)[a,b]	−1.0	−0.9	−0.9	136.9
6P $H_{\beta'}$	−3.0 (−3.2)[a,b]	−2.7	−2.4	−2.4	136.9
7P H_α	7.4 (8.7)[a,b]	7.9	8.0	8.4	−28.4
7P $H_{\alpha'}$	3.6 (4.0)[a,b]	3.9	4.1	4.1	−28.4
7P H_β	−3.5 (−3.4)[a,b]	−3.2	−3.0	−2.4	−103.6
7P $H_{\beta'}$	−4.4 (−4.3)[a,b]	−4.1	−3.7	−2.8	−103.6
2V H_α	6.8		6.9		
2V H_β	1.8, 0.8[c]		1.6, 0.7[c]		
4V H_α	5.8		6.1		
4V H_β	0.2, 0.9[c]	0.3, 0.9[c]	0.4, 1.0[c]		126.3
α-*meso*-H	−3.2				
β-*meso*-H	6.3		6.7		
γ-*meso*-H	−4.9 (−4.6)[a]		−3.8		
δ-*meso*-H	9.4		9.5		
Ser-40	23.5, −7.0, −7.2			22.6, −5.6	
Ile-120				0.1, −0.9, −2.8	

[a] Chemical shift of minor species (see the text) given in parentheses. At least two different minor species are involved, and probably three (see the text). [b] Propionate α- and *β*-protons labeled as α or α′ and *β* or *β*′, respectively, on the basis of relative chemical shift. No stereochemical information is implied. [c] Vinyl *β*-protons could not be assigned with regard to cis and trans.

Table 2: NP2−ImH ^{1}H and ^{13}C Heme Assignments in D_2O at pH 7.0 at Two Temperatures

	^{1}H resonance (ppm)		^{13}C resonance (ppm)
substituent	20 °C	30 °C	20 °C
3Me	15.7	15.6	−40.0
5Me	12.8	12.5	−26.0
1Me	11.7	11.5	−19.5
8Me	1.1	1.9	−5.5
6P H_α	13.6, 12.0	12.9, 11.8	−44.3
6P H_β	−1.4, −3.0	−1.2, −2.8	132.0
7P H_α	8.9, 4.6	9.4, 4.9	−29.5
7P H_β	−3.0, −3.8	−2.8, −3.3	108.0
2V H_α	6.7		
2V H_β	1.8, 1.2		
4V H_α	6.1		
4V H_β	1.2, 0.7	1.5, 0.9	128.5
α-*meso*-H	−2.7	−1.9	46.7
β-*meso*-H	7.5	7.7	19.5
γ-*meso*-H	−4.6	−3.9	42.2
δ-*meso*-H	9.8	9.9	18.4
Ser-40	21.9, −5.8, −5.9	21.5	24.8
Ile-120	0.0, −1.0, −3.0	0.3, −0.8, −2.9	10.1

bound to the Fe(III) heme center, by observation of chemical exchange cross-peaks in the NOESY spectrum between the free and bound ligand of a sample containing a slight excess of NMeIm over NP2 (not shown). The other three of these methyl resonances are due to the 5-, 1-, and 3-heme methyls, respectively, based upon the NOE connectivities found in the WEFT-NOESY spectrum (Figure 5). The fourth heme methyl (8Me) is found in the diamagnetic region at 0.6 (^{1}H) and −4.6 ppm (^{13}C). There is also a small peak, seen in the

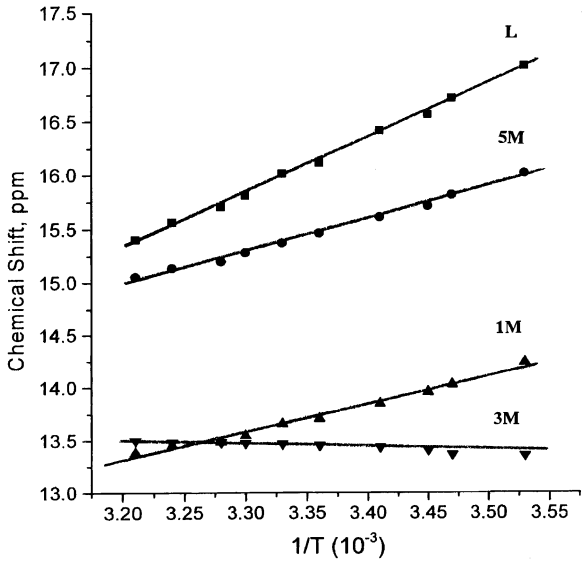

FIGURE 3: Curie plot of the four heme methyl resonances of the NP2−NMeIm complex.

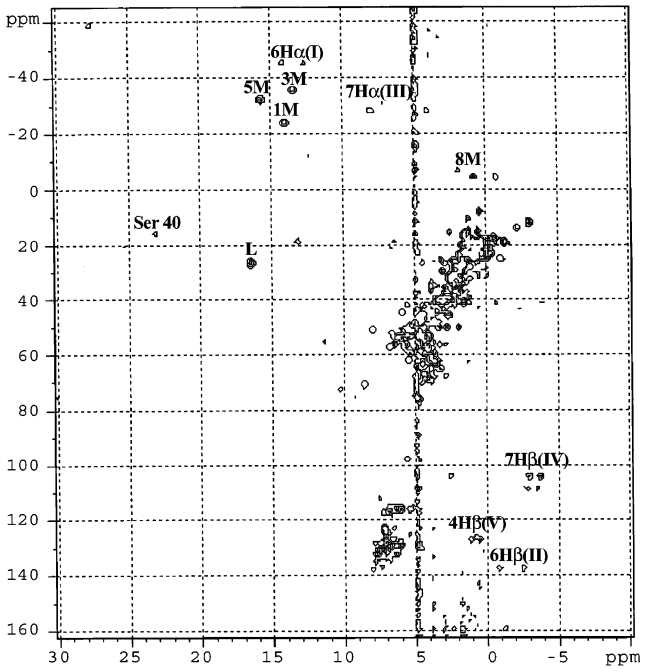

FIGURE 4: HMQC map of the NP2−NMeIm complex at 20 °C and 500 MHz.

1D spectrum of Figure 1B at 29 ppm (intensity ∼10% of that of the methyl resonances in the 13−18 ppm region) and in the HMQC map (Figure 4) at 27.5 (^{1}H) and −59 ppm (^{13}C) that, by its cross-peak intensity, appears to be a methyl group. Because of its chemical shifts in both the ^{1}H and ^{13}C dimensions, it undoubtedly is a heme methyl, which therefore suggests that there is a minor heme orientational isomer (orientation A, Scheme 1). However, we have been unable to find additional resonances that can be shown unambiguously also to be due to such a minor heme orientational isomer, and it thus remains unassigned. If it is a heme methyl of the minor orientational isomer, then it is likely that the other three heme methyl resonances of this isomer are buried in the diamagnetic protein envelope, for there are no obvious additional HMQC peaks outside that region. Further experiments will be required to assign this small peak. In the

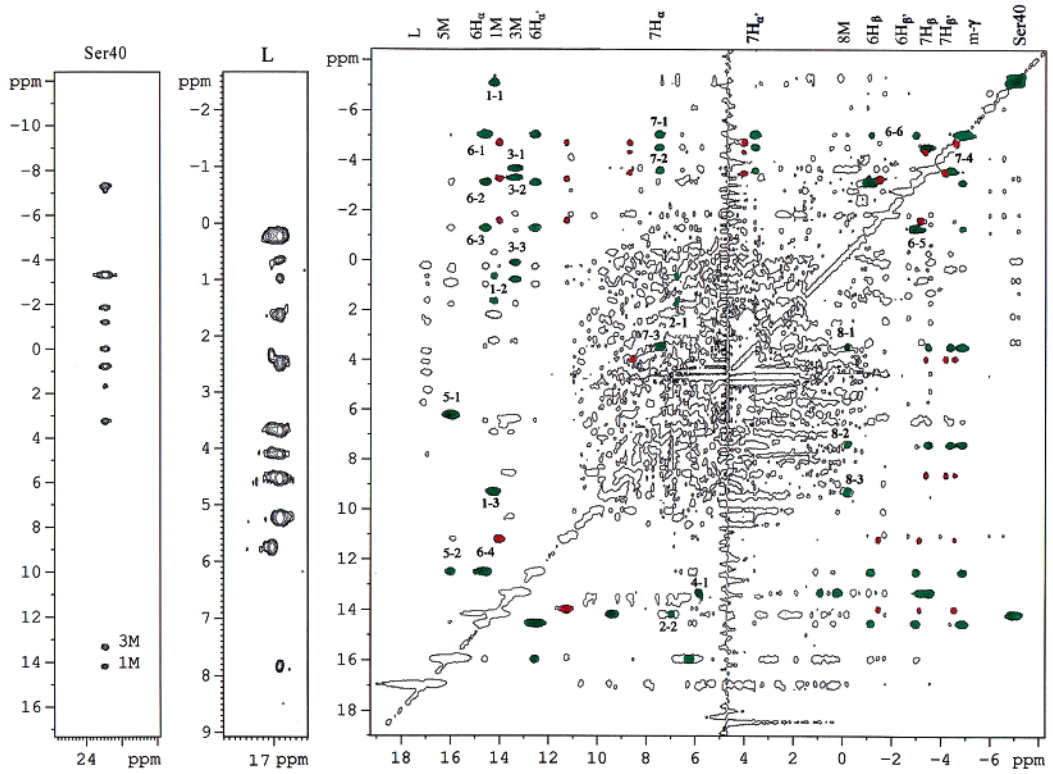

FIGURE 5: WEFT-NOESY map of the NP2−NMeIm complex at 10 °C and 500 MHz. The mixing time was 30 ms. The cross-peak labels represent the following: 1-1, 1Me−Ser-40; 1-2, 1Me−2H$_\beta$; 1-3, 1Me−*meso* δ; 2-1, 2H$_\alpha$−2H$_\beta$; 2-2, 2H$_\alpha$−1Me; 3-1, 3Me−Ile-120 Me; 3-2, 3Me−*meso* α; 3-3, 3Me−4H$_\alpha$; 4-1, 4H$_\alpha$−3Me; 5-1, 5Me−*meso* β; 5-2, 5Me−6H$_\alpha$; 6-1, 6H$_\alpha$−*meso* γ; 6-2, 6H$_\alpha$−6H$_{\beta'}$; 6-3, 6H$_\alpha$−6H$_\beta$; 6-4, 6H$_\alpha$−6H$_{\alpha'}$; 6-5, 6H$_\beta$−6H$_{\beta'}$; 6-6, 6H$_\beta$−*meso* γ; 7-1, 7H$_\alpha$−*meso* γ; 7-2, 7H$_\alpha$−7H$_{\beta'}$; 7-3, 7H$_\alpha$−7H$_{\alpha'}$; 7-4, 7H$_\beta$−7H$_{\beta'}$; 8-1, 8Me−7H$_{\alpha'}$; 8-2, 8Me−7H$_\alpha$; and 8-3, 8Me−*meso* δ. Cross-peaks marked in green are for the major isomer, and those marked in red are for the minor isomer.

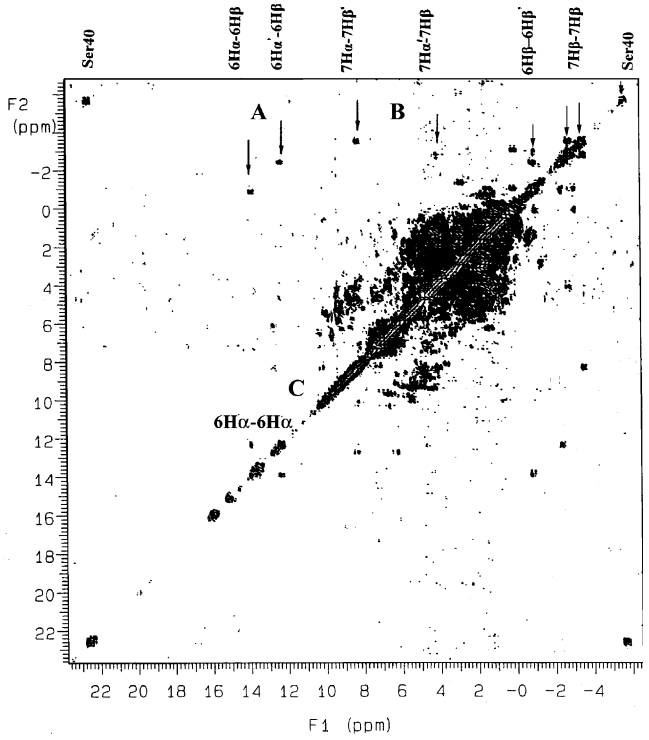

FIGURE 6: DQF-COSY map of the NP2−NMeIm complex at 30 °C and 300 MHz.

HMQC map (Figure 4), there are also strongly coupled proton pairs at 12.6 and 14.0 ppm (^{1}H) and −45.5 ppm (^{13}C) (labeled I in Figure 4 and A in Figure 6) that, together with the DQF-COSY spectrum of Figure 6, can be identified as those of the 6-propionate α-CH$_2$, −2.7 and −1.0 ppm (^{1}H) and 136.9 ppm (^{13}C) (labeled II in Figure 4 and A in Figure 6, 6-propionate β-CH$_2$), 7.9 and 3.9 ppm (^{1}H) and −28.4 ppm (^{13}C) (labeled III in Figure 4 and B in Figure 6, 7-propionate α-CH$_2$), −3.2 and −4.1 ppm (^{1}H) and 103.6 ppm (^{13}C) (labeled IV in Figure 4 and B in Figure 6, 7-propionate β-CH$_2$), and 0.3 and 0.9 ppm (^{1}H) and 126.3 ppm (^{13}C) (labeled V in Figure 4, 4-vinyl β-CH$_2$). There should be a sixth strongly coupled proton pair, due to 2-vinyl β-CH$_2$; it is buried in the protein envelope, and cannot be detected in the HMQC map, but the proton resonances are clearly observed at 1.6 and 0.7 ppm in the NOESY map of Figure 5, along with that of the 2-vinyl α-CH (6.9 ppm), and the corresponding 4-vinyl α-CH resonance is at 6.1 ppm (Figure 5).

The pattern of three resolved heme methyl resonances (due to 3-, 5-, and 1Me, respectively) for the imidazole complex is somewhat different (15.6, 12.5, and 11.5 ppm, respectively, at 30 °C), as shown in Figure S1 for the 1D ^{1}H spectrum and in Figure S2 for the HMQC spectrum (Supporting Information), and again, the ^{13}C resonances are also somewhat different in chemical shift, as summarized in Table 2. On the basis of the HMQC spectrum, the fourth heme methyl resonance of the imidazole complex (8Me) is found at 1.9 ppm at 30 °C. All heme substituent resonances for the NP2−NMeIm and NP2−ImH complexes were assigned, as described in detail in the Supporting Information. The assignments are listed in Tables 1 and 2, respectively.

The *N*-methyl peak of the coordinated NMeIm ligand shows two signals in a roughly 3:1 intensity ratio, shown in

expanded form in the inset of Figure 1B, where the two resonances are seen at 16.9 and 17.0 ppm, respectively, at 10 °C. Each of these two *N*-methyl resonances has NOEs to some of the same, and some different, protein residues, as shown in the 17 ppm region expanded strip of the NOESY spectrum of Figure 5. We believe that these two sets of cross-peaks represent two seatings of the NMeIm ligand, with the *N*-methyl group pointing in the two possible directions, assuming a fixed orientation of the ligand plane. Ile-120, Leu-122, and Leu-132 are all close enough to where the NMeIm methyl group would be in one of the seatings (*15*) (Scheme 1, orientation B) that they should provide steric contact with the *N*-methyl group when it points into the pocket, thus preventing its rotation. That, coupled with the lack of an NH group to provide hydrogen bonding stabilization of the orientation of the NMeIm ligand, could easily produce two orientations of the *N*-methyl group. [A similar two-seatings situation is observed for the iodine atom of 4-iodopyrazole (4IPzH) in the NP1−4IPzH complex, but in the NP4−4IPzH complex the position of the iodine is ordered and hence there is only one orientation (*39*).] Thus, it could be that the rate of chemical exchange between the two seatings of the NMeIm ligand is too slow to be detected on the NMR time scale at 10 °C. The second, weaker signal, observed at 10 and 20 °C, is not observed at the higher temperatures used in this NMR investigation (25−37 °C).

There are several hyperfine-shifted proton resonances in the ^{1}H NMR spectra of the NP2−NMeIm complex that are due to protein residues that are very close to the heme center. These include the four-spin system C (6.2, 8.2, 10.0, and 12.7 ppm) observed in the DQF-COSY map of Figure 6, which we believe is due to the aromatic ring of Phe-66. In addition, the DQF-COSY spectrum at 30 °C (Figure 6) shows an apparent two-spin system at 22.6 and −5.6 ppm [although there are two very closely spaced resonances at −5.6 ppm, as revealed in the NOESY spectrum of Figure 5 (23.5, −7.0, and −7.2 ppm at this temperature), which makes this a three-spin system]. There are also NOEs (Figure 5) between one of these protons and 1Me, as well as between the proton at 23.5 ppm and both 3-M and 1-M, as shown in the 23.5 ppm region of the NOESY spectrum of Figure 5. The best candidate for this assignment is the spin system of Ser-40, the β-carbon of which is 6.5 Å away from 1Me and 4.7 Å from 3Me (*15*). The difference in chemical shift of the two β-CH_2 protons of this protein side chain (23.5 and −7.2 ppm) is one of the largest reported chemical shift differences for two geminal protons, and it can only result from a very specific orientation of that geminal pair of protons, which creates extremely different dipolar (pseudocontact) shifts for the two, with one being very close to the heme iron and in the region of space where the dipolar shift is large and positive [small distance r and small angle θ, making the tetragonal dipolar shift geometric term $(3\cos^2\theta - 1)/r^3$ large and negative (*24*, *59*)], while the other is further away and at an angular orientation that places it in the relatively small negative dipolar shift regime.

The other apparently three-spin system (−0.1, −0.9, and −2.8 ppm at 30 °C, Figure 6) has NOE connectivity with 3Me (Figure 5). This system cannot be mistaken for a heme vinyl group, because of the intensity of the peak at −2.8 ppm, which identifies it as belonging to a methyl group. The closest residue to 3Me having a methyl group is Ile-120 (3.9 Å), but it should be a six-spin system. It is likely that not all *J*-coupled protons exhibit cross-peaks under the conditions appropriate for optimizing the *J* couplings and NOEs of paramagnetically shifted heme resonances (WEFT sequence, which effectively nulls proton signals with long relaxation times, as well as short acquisition times and relaxation delays smaller than those used for diamagnetic proteins).

Heme Methyl Resonance Pattern and Orientation of the Nodal Plane of the Orbital Utilized for Spin Delocalization in the Low-Spin NP2 Complexes. The order of heme methyl resonances for the two axial ligand complexes of NP2 is different: 5 > 3 > 1 > 8 for the NMeIm complex below 30 °C, but 5 > 1 > 3 > 8 above 30 °C, and 3 > 5 > 1 > 8 for the ImH complex at all temperatures. In previous work, we showed that the order and spacing of the heme methyl and *meso*-H resonances could be predicted by considering the effect of the orientation of the axial ligand nodal plane (usually the proximal histidine imidazole plane) on the contact and dipolar contributions, as well as the effect of the vinyl substituents of protohemin, to the chemical shift of these groups (*38*). In that work, the contact contribution was estimated from Hückel calculations and the dipolar shift was estimated from the *g* anisotropy, in combination with the concept of counter-rotation of the **g** tensor with rotation of the axial ligand nodal plane (*40*). A modified plot of the angular dependence of the heme methyl shifts for heme *b* containing low-spin ferriheme proteins on the orientation of the nodal plane of the axial ligand(s) is shown in Figure 7A, and a program for plotting spectra as a function of angle is available on our Web site (*41*). In this modified plot, the numerical values for the predicted chemical shifts (*38*) have been removed so that the plot is more general and is independent of the effect of donor strength of the other ligand and/or of histidine imidazole N−H hydrogen bonding or deprotonation. Thus, in Figure 7A, only the predicted order and relative spacing of the heme methyl resonances are considered. However, the relationship for low-spin ferrihemes to the approximate extension of the diamagnetic region of the protein resonance envelope (0−10 ppm) is marked in yellow to indicate the point at which the methyl signals of low-spin ferriheme proteins become unresolved in 1D ^{1}H NMR spectra of heme proteins.

Upon application of the plot of Figure 7A to the heme methyls of the NP2−NMeIm and NP2−ImH complexes, the order of the resonances of the NMeIm complex (5 > 3 > 1 > 8), the close spacing of the 1Me and 3Me resonances, and their crossover at higher temperatures indicate that the nodal plane of the heme 3e(π) orbital utilized for spin delocalization is at 162 ± 2°, and varies slightly with temperature, while for the ImH complex (3 > 5 > 1 > 8), that nodal plane is oriented at ∼150−155° (Figure 7A). Since the crystal structure shows that the imidazole ring of His-57 is positioned at ∼130−135° (*15*) (Scheme 1, B orientation) or at exactly 135°, based on the high-spin NP2 ^{1}H NMR spectrum, as discussed below, the angles obtained from the heme methyl resonance order and spacing indicate that the exogenous imidazole ligand exerts at least an equal, and probably a greater, influence on the orientation of the nodal plane of the heme as does His-57, and it is thus clear that the two exogenous ligands of this study do not have the same orientation. If the influence of the two axial ligands in a given complex is equal, then we expect that the angular orientation

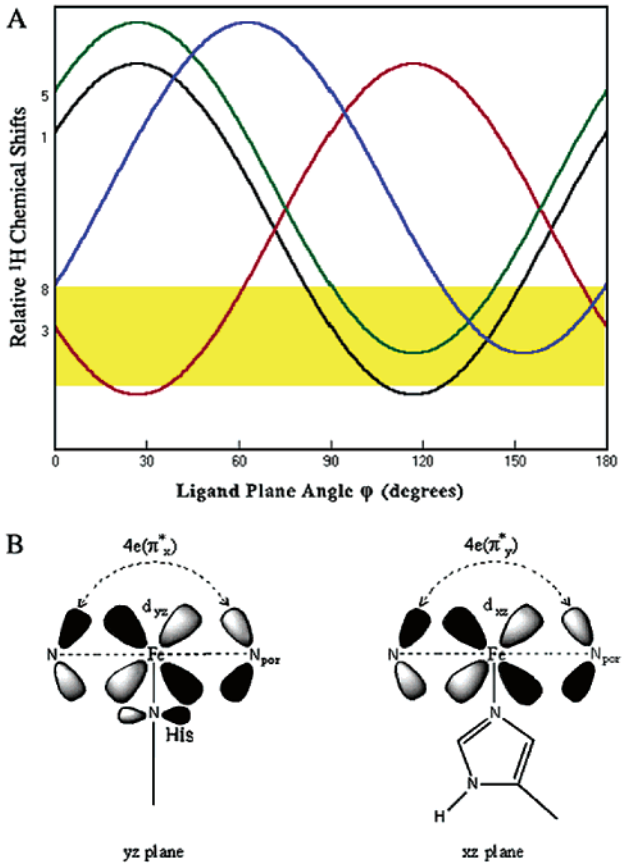

FIGURE 7: (A) Dependence of heme methyl shifts on the axial ligand nodal plane orientation angle φ for low-spin ferrihemes (adapted from ref *38*). The angle φ is defined in Scheme 1. No chemical shifts are provided on this modified plot, which is thus generically applicable to any high- or low-spin histidine-ligated heme protein, although the approximate end of the protein diamagnetic resonance envelope that is appropriate for low-spin ferrihemes is marked; for high-spin Fe(III) proteins, the observed methyl shift pattern is that of the angle that is 90° shifted from the known axial ligand plane orientation (see the text). (B) Iron d_{xz} and d_{yz}, axial ligand π or π^* orbital on the binding nitrogen, and porphyrin $4e(\pi^*_x)$ and $4e(\pi^*_y)$ orbital interactions for high-spin ferrihemes. The transfer of the d_{yz} spin density is to the histidine π or π^* orbital, while the transfer of the d_{xz} spin density is to the $4e(\pi^*_y)$ porphyrin orbital.

of the nodal plane of the heme orbital utilized for spin delocalization will be the average of those of the two ligands, and with this assumption, we conclude that the NMeIm ligand must have its nodal plane aligned at 189−194°, or 9−14° clockwise from the nitrogens of pyrrole rings II and IV in the B orientation of Scheme 1, while the ImH ligand must have its plane aligned at 170−180°. The orientation of the imidazole plane of the NP4−ImH complex for the B heme orientation (Scheme 1) of NP2 is ∼170° (*18*), in good agreement with the lower end of this range, assuming that the orientation of the imidazole plane is the same in the NP2−ImH complex as it is in the B isomer of the NP4−ImH complex. However, the imidazole ligand in the NP4−ImH complex is hydrogen bonded to a water molecule that is in turn hydrogen bonded to the OH group of Thr-121 (*18*), which is not present in NP2, but rather is replaced with a bulky isoleucine residue, Ile-120 (*15*).

If the exogenous ligand exerts a more important influence on the orientation of the nodal plane of the His-57 ligand, then the orientation of the exogenous ligand is given by the angles determined from the plot of Figure 7A, 150−155°, which is in much poorer agreement with the crystal structure of the NP4−ImH complex for the B heme orientation (Scheme 1) (*18*). However, considering the NP2 L122,132V distal pocket mutants, which have porphyrin nodal planes aligned at up to 168°, yielding dihedral angles of the His-57 and ImH planes of up to 60°, while the EPR spectra are consistent with the ligands being in "parallel" planes (*43*), suggests that the exogenous imidazole ligand contributes more strongly to the orientation of the porphyrin nodal plane than does His-57. On the basis of this argument, it appears that ImH contributes more strongly to determining the orientation of the nodal plane of the $3e(\pi)$ orbital of the heme that is used for spin delocalization, and that the large Ile-120 residue in the distal pocket of NP2 may play a steric role in determining the orientation of the exogenous ligand, in comparison to the hydrogen bonding role played by Thr-121 of NP4 (*16*).

With NMeIm as an adduct, there is no nitrophorin crystal structure available. An orientation of the plane of NMeIm 9−14° clockwise of the N−Fe−N axis of pyrrole rings II and IV in the B orientation of Scheme 1 would place it very tightly sandwiched between the bulky side chains of Ile-120 and Leu-132 (*15*), which seems much less likely than taking up the space provided between Leu-122 and Ile-120 (Scheme 1, orientation B), for which an axial ligand plane orientation of approximately 162° is eminently reasonable. Whatever its true orientation, it can certainly be expected to be held in place, in one of the possible seatings related by a 180° rotation of the ligand, by the trio of bulky residues on the distal side of the heme, Ile-120, Leu-122, and Leu-132 (*15*). The EPR spectrum of the NP2−NMeIm complex is rhombic, with *g* values of 3.02, 2.26, and 1.37 (*42*), indicative of a parallel ligand orientation, such as the dihedral angle of 27° that would result from the assumption that NMeIm determines the orientation of the nodal plane of the π orbital of the porphyrin ring that determines the isotropic shifts of the heme substituents. Crystal structures of the NP2−NMeIm and NP2−ImH complexes should be determined to answer definitively the question of the orientation of the exogenous ligands in these complexes.

Assignment of Heme Substituent Resonances of High-Spin NP2. As mentioned above, the 1D proton NMR spectrum of the NP2 high-spin complex (Figure 1A) contains well-resolved proton resonances that are shifted far from the diamagnetic region. To assign these proton resonances, we utilized two methods. The first was 1D saturation transfer difference spectroscopy, which depends on chemical exchange between the high-spin form of NP2 and its low-spin NMeIm complex at 37 °C. (The same cannot be accomplished using the ImH complex, because the rate of ligand exchange in that case is too slow.) The sample utilized in this experiment contained only enough NMeIm to complex approximately 20−30% of the protein present at this temperature. Under these conditions, because chemical exchange of NMeIm is sufficiently rapid at 37 °C, 1D saturation transfer difference experiments (Figure 8) allowed assignment of the four methyl groups, as well as the geminal α-propionate protons of the high-spin protein. It is particularly interesting to note that irradiation of the large methyl signal at 65 ppm led to two connections to low-spin methyls

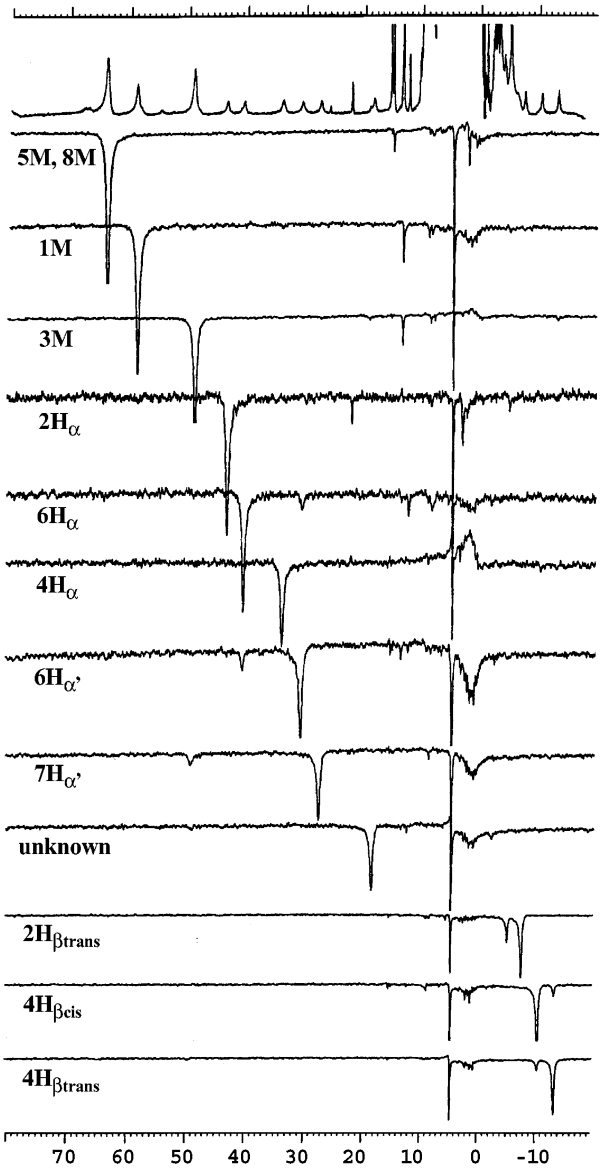

FIGURE 8: 1D ^{1}H saturation transfer of a mixture of NP2 and the NP2−NMeIm complex at 37 °C and 500 MHz.

through saturation transfer, one at 15 ppm and the other at 2 ppm. The 15 ppm methyl signal has already been assigned above to the 5-methyl of the heme, and the peak at 2 ppm is the 8-methyl, which is shifted somewhat from its position at −0.2 ppm at 10 °C and −0.6 ppm at 20 °C. (This resonance was not unambiguously identified at 30 °C.) Hence, the 5- and 8-methyl signals of the high-spin form of NP2 both occur at 65 ppm at 37 °C. The small peaks at 69, 68, and 56 ppm appear to be due to the methyl resonances of the A heme rotational isomer (Scheme 1); not surprisingly, the existence of this small amount (∼8−10%) of the A heme rotational isomer was not detected in the X-ray crystal structure of NP2 (*15*). The fourth heme methyl resonance of this isomer could not be detected, but is probably buried under either the peak at 60 ppm or the peak at 50 ppm. Attempts to assign these minor heme methyl signals by 1D saturation transfer or NOE difference spectroscopy were unsuccessful.

Although the order of 1Me and 3Me of the NMeIm complex is reversed when the temperature is increased above

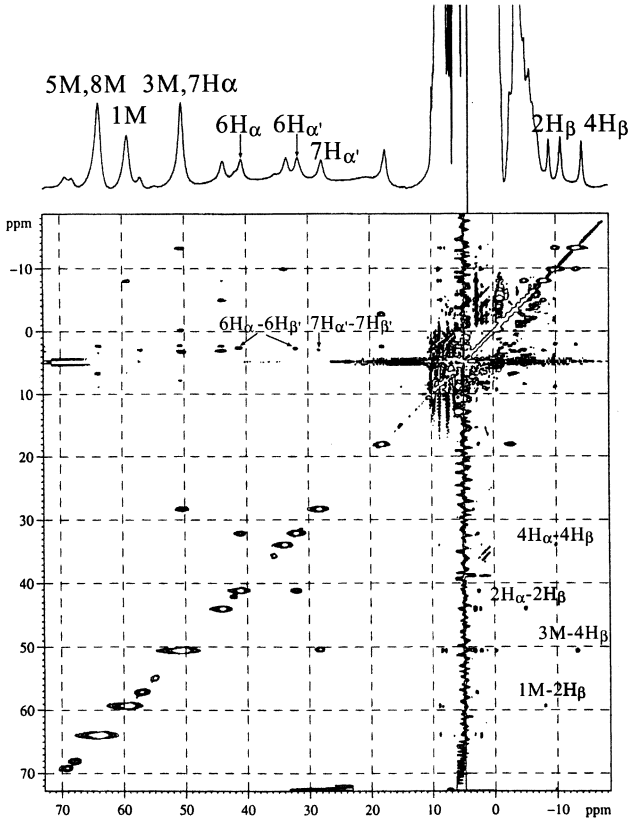

FIGURE 9: WEFT-NOESY map of high-spin NP2 at 20 °C and 500 MHz. The mixing time was 12 ms.

∼30 °C (Figure 2), the order of the heme methyl groups of the B heme orientational isomer (Scheme 1) of the high-spin protein remains the same throughout the temperature range that has been investigated (8 = 5 > 1 > 3), although for all of the L122 and L132 distal pocket mutants at 10 °C, a small splitting between the 8 and 5 resonances was observed, with shifts of 8 > 5 in all three cases (*43*). Another interesting feature of Figure 8 is the fact that several NOEs are also detected, most notably between the geminal CH_α atoms of the propionate groups. This is not surprising, because the saturation transfer and 1D NOE experiments are carried out identically; only the strong geminal proton NOEs are observed, indicating that they arise from spin diffusion. These include the β-vinyl and β-propionate resonances.

The second method utilized for assignment of the heme substituent resonances was a NOESY spectrum of the high-spin NP2 protein. In Figure 9 is shown the NOESY spectrum of NP2 at pH 7.0 and 20 °C in the absence of any added ligand. On the basis of the assignment of the heme methyl resonances accomplished by the saturation transfer measurements shown in Figure 8, the propionate and vinyl resonances could be assigned from these NOESY spectra. Clear NOEs are seen between 2V H_α at 44.1 ppm and 2V $H_{\beta cis}$ at −4.8 ppm, and in turn between 2V $H_{\beta cis}$ and 2V $H_{\beta trans}$ at −7.9 ppm. Similar connectivities are found for 4V H_α at 34 ppm and 4V $H_{\beta cis}$ at −9.8 ppm, and for 4V $H_{\beta cis}$ and 4V $H_{\beta trans}$ at −13.2 ppm. Likewise, the 6- and 7-propionate Hα resonances are correlated to their respective H_β resonances in the NOESY spectrum of Figure 9, except for one each of the 6- and 7P-H_β resonances, which could not be unambiguously assigned. The results are summarized in Table 3.

Table 3: High-Spin NP2 Heme Resonance Assignments at 20 °C and pH 7.0

substituent	^{1}H chemical shift (ppm)	substituent	^{1}H chemical shift (ppm)
8Me	63.8	2V $H_{\beta cis}$	−4.8
5Me	63.8	2V $H_{\beta trans}$	−7.9
1Me	59.5	6P H_{α}	41.2
3Me	50.6	6P $H_{\alpha'}$	32.1
7P H_{α}	50.6	6P H_{β}	2.7
7P $H_{\alpha'}$	28.4	6P $H_{\beta'}$	*a*
7P H_{β}	3.1	4V H_{α}	34.0
7P $H_{\beta'}$	*a*	4V $H_{\beta cis}$	−9.8
2V H_{α}	44.1	4V $H_{\beta trans}$	−13.2

[a] Could not be unambiguously assigned.

Unfortunately, the *meso*-H resonances of NP2 could not be detected, although there are several broad resonances in the 55−20 ppm region that could be due to the four *meso*-H protons. As a guide as to where these resonances might occur, the chemical shift of the *meso*-H of OEPFeCl in DMSO-d_6 at 21 °C is 42 ppm (*24*). The bis-DMSO complex is a six-coordinate high-spin ferriheme center, as are the nitrophorins in the absence of added ligand, where a water molecule is bound to the heme iron, and thus, except for the effect of the axial histidine imidazole plane, we should expect the *meso*-H resonances to be centered around 42 ppm or so at ambient temperatures. The *meso*-H chemical shifts of most high-spin ferriheme proteins have not been reported; however, Rae and Goff report those of the lactoperoxidase heme peptide in DMSO to be in the range of 34−40 ppm at 25 °C and those of protoporphyrin IX in DMSO to be in the range of 37−41 ppm at 25 °C (*44*). La Mar and co-workers report the *meso*-H resonances of wild-type sperm whale metmyoglobin and several of its valine E11 mutants to be at ∼40 ppm (*30*), while in contrast, these authors report that *Aplysia* methemoglobin and several mutants of sperm whale metmyoglobin, in which the distal E7 histidine has been mutated to several residues that are not capable of stabilizing the binding of water through H-bond acceptance, have their *meso*-H resonances in the −20 to −40 ppm region (*30*). The spin-admixed $S = {}^3/_2, {}^5/_2$ ferriheme center of *Rhodopseudomonas palustris* cytochrome *c*′ has the *meso*-H resonances between −11.9 and −21.8 ppm at 40 °C (*33*); the negative chemical shifts are indicative of five-coordinate ferriheme centers (*24*, *30*), whereas for the six-coordinate ferriheme NP2 aquo complex, we expect the *meso*-H shifts to be near 40 ppm but possibly to be individually shifted due to the effect of the nodal plane of the proximal ligand. We have not succeeded in unambiguously assigning these *meso*-H resonances, although three broad one-proton resonances are clearly seen in the 1D spectrum of the NP2 L122,132V double mutant between 30 and 40 ppm (*43*). Nevertheless, all other heme substituent resonances except two β-CH resonances of the propionate groups of the high-spin form of NP2 have been assigned, and those assignments are listed in Table 3.

Relationship of Heme Methyl Resonance Patterns in High-Spin Ferriheme Proteins to the Histidine Imidazole Plane Orientation. The order of heme methyls for high-spin NP2 (8 = 5 > 1 > 3, with methyl shifts ranging from 65 to 51 ppm at 20 °C) is different from that of horseradish peroxidase (5 > 1 > 8 > 3, with methyl shifts ranging from ∼80 to ∼50 ppm at 40 °C) (*34*, *35*), metmyoglobin (8 > 5 > 3 > 1, with methyl shifts ranging from ∼92 to ∼53 ppm at 25 °C for sperm whale metMb and from 102 to 56 ppm at 25 °C for elephant metMb species A or from 72 to 48 ppm for species B) (*29*), *Rh. palustris* and *Rhodocyclus gelatinosus* ferricytochrome *c*′ (8 > 1 > 5 > 3, with shifts ranging from ∼80 to ∼60 ppm at 45 °C), and metlactoperoxidase (8 > 5 > 3 > 1, with shifts ranging from ∼70 to ∼46 ppm at 25 °C) (*44*). Thus, NP2 has a unique pattern of heme methyl resonances as compared to other high-spin heme proteins investigated thus far. The assignments, chemical shifts, average chemical shift, and spread of the methyl resonances of the high-spin ferriheme proteins whose methyl resonances have been assigned are listed in Table 4, where it can be seen not only that the order of heme methyl resonances differs among the types of high-spin ferriheme proteins but also that the average chemical shift and the spread of the methyl resonances differ among these proteins. NP2 has not only a unique order but also the smallest average and smallest spread of heme methyl resonances among the proteins that are listed.

We have considered the patterns of heme resonances for the high-spin heme proteins whose heme methyl peaks have been assigned, and attempted to determine whether there is a relationship between the orientation of the axial histidine plane in these ferriheme proteins and the order of heme methyl resonances, of the type shown in Figure 7A (*41*) that exists for low-spin ferriheme proteins (*38*). Using the same axis system (Scheme 1), in which the *x*-axis passes through the nitrogens of pyrrole rings IV and II, and angles are measured in a counterclockwise direction for the A orientation (clockwise direction for the B orientation) (*38*), the following histidine imidazole plane angles are observed in the protein crystal structures: 178° for met-Mb (*45*−*47*), 95° for HRP (*48*, *49*), and 130−135° for NP2, very near the *meso*-β,δ line of the heme (*15*). The crystal structures of several of the cytochromes *c*′ have been reported (*50*−*56*), and in all cases, the Cys-X-Y-Cys-His sequence near the C-terminus of the protein to which the heme is bound also has the histidine imidazole plane aligned very near the *meso*-β,δ line of the heme, an angle of ∼135°.

In Table 4 are presented the chemical shifts and order of heme methyl resonances of each of these proteins in its high-spin form, as well as those of three distal pocket mutants of NP2 (*43*), and a summary of the order of methyl resonances found in the low-spin forms of each of the proteins except the cytochromes *c*′. From a cursory perusal of the patterns presented in Table 4, it appears that the order of heme methyl resonances more or less reverses upon going from the high-spin to the low-spin state. More specifically, using the plot shown in Figure 7A (*41*), which was developed for low-spin heme proteins having at least one histidine ligand (*38*), for which it was suggested that the orientation of the nodal plane of the histidine imidazole ligand determined the orientation of the nodal plane of the porphyrin 3e(π) orbital utilized for spin delocalization via porphyrin to Fe π donation (*38*), we find that for HRP, NP2 and its distal pocket mutants, and the metmyoglobins the order of heme methyl resonances is close to that predicted for a 90° rotation of the porphyrin nodal plane as compared to the known orientation of the axial ligand plane. For example, for HRP, with the histidine imidazole plane oriented at ∼95° based upon the crystal structure of related proteins (*48*, *49*), the order of heme

Table 4: Heme Methyl Shifts of High-Spin and Low-Spin States of Several Heme Proteins

protein	*T* (°C)	histidine nodal plane angle (deg)	HS Me order	apparent nodal plane angle (deg)	chemical shift (ppm)						LS Me order	LS Me spread (ppm)
					8Me	5Me	3Me	1Me	av	spread		
protohemin[a]	25	none	8 > 5 > 3 > 1	none	63.2	62.2	57.7	54.4	59.4	9.8	8 > 5 > 3 > 1[b]	4.7
SW met-Mb[c]	25	165[d]	8 > 5 > 3 > 1	~73	91.7	84.9	73.2	53.2	76.1	38.5	5 > 1 > 8 > 3[e]	22.2
El met-Mb, sp. A[c]	25	165?[d]	8 > 5 > 3 > 1	~73	102.1	90.5	76.4	56.1	81.3	46	5 > 1 > 8 > 3[f]	19.4
El met-Mb, sp. B[c]	25	165?[d]	8 > 5 > 3 > 1	~73	71.5	69.1	62.8	47.9	61.1	23.6	5 > 1 > 8 > 3[f]	19.4
Cyt *c*′[g]	40	~135	8 > 1 > 5 > 3	~55−65	81.0	68.6	61.6	76.5	71.9	19.4	*h*	
HRP[i]	50	95	5 > 1 > 8 > 3	~0	80	72	65	52	67	28	8 > 3 > 5 > 1[j]	27[k]
NP2[l]	15	135[m]	8 = 5 > 1 > 3	45	64.3	64.3	59.2	50.1	59.5	14.2	3 > 5 > 1 > 8[l]	14.5[l]
L122V NP2[m]	15	136[m]	8 > 5 > 1 > 3	45−50	67.7	67.1	52.8	60.0	61.9	14.9	3 = 5 > 1 > 8[m]	10.7[n]
L132V NP2[m]	15	137[m]	8 > 5 > 1 > 3	45−50	67.7	67.1	52.8	60.0	61.9	14.9	5 > 1 > 3 > 8[m]	12.1[n]
L122,132V NP2[m]	15	138−139[m]	8 > 5 > 1 > 3	45−50	67.6	65.8	53.2	59.0	61.4	14.4	5 > 1 > 3 > 8[m]	9.9[n]

[a] From ref *65* (DMSO-d_6). [b] From ref *66*. [c] From ref *29*. [d] From ref *57*. [e] From ref *67*. [f] From ref *68*. [g] From ref *33*. [h] Not available. Complex does not form. [i] From ref *35*. [j] From ref *69*. [k] Measured at 35 °C. [l] From this work. [m] From ref *43*. [n] Imidazole complex. From ref *43*.

methyl resonances for the high-spin form (5 > 1 > 8 > 3) is that predicted for a porphyrin nodal plane oriented at ~0−10°, while for NP2, with its histidine imidazole plane oriented at ~130−135° based on the crystal structure (*15*), the order and relative spacing of the heme methyl resonances (8 = 5 > 1 > 3) are those predicted for a porphyrin nodal plane oriented at exactly 45° (the angle at which the 8-M and 5-M resonances cross). For sperm whale metmyoglobin, with the histidine imidazole plane oriented at 178° (−2°) (*45*−*47*), however, the order and relative spacing of the heme methyl resonances (8 > 5 > 3 > 1) are those predicted for a heme nodal plane oriented at ~73°, or roughly 15° away from the angle of 90° predicted by the orientation of the histidine imidazole plane in the crystal structures done recently, mainly by molecular replacement, often using low-spin met-Mb structures as the starting point (*45*−*47*). If one looks at the original sperm whale myoglobin structure (*57*), however, the axial histidine imidazole plane is ~15° clockwise from the $N_{II}-N_{IV}$ axis, at an angle of ~165° (*57*), in agreement with the 90° rotation of the nodal plane of the high-spin ferriheme π orbital described above.

If we assume that this apparent 90° shift in the porphyrin nodal plane angle of the orbital involved in spin delocalization as compared to the histidine imidazole nodal plane angle continues to hold up for additional high-spin heme proteins in addition to those listed in Table 4, then an explanation for this phenomenon must be found in terms of the bonding interactions in the high-spin ferriheme protein. It has been shown previously that high-spin ferrihemes have large positive chemical shifts of all pyrrole substituents due to equal σ symmetry spin delocalization to all β-pyrrole positions because of half-occupation of the $d_{x^2-y^2}$ orbital (*24*, *58*, *59*). In addition, high-spin ferrihemes also have an unpaired electron in each of the other four d orbitals. It is expected that the d_{z^2} and d_{xy} unpaired electrons cannot lead to significant spin delocalization, based on symmetry and electron density considerations, but the unpaired electrons in the d_{xz} and d_{yz} orbitals can be involved in π spin delocalization to the porphyrin ring that will add an additional shift to the proton resonances of heme substituents except for protons that are directly bound to the aromatic porphyrin ring (in this case, the shifts due to π delocalization *subtract* from those due to σ delocalization) (*24*, *58*, *59*). Since each of these latter d orbitals has a nodal plane perpendicular to the heme plane, and the nodal planes of the two are oriented at 90° angles to each other, the d_{xz} and d_{yz} orbitals provide the only means by which the level of π spin delocalization to the heme can be increased or decreased at various β-pyrrole positions. Hence, the isotropic shifts of high-spin ferriheme systems are a combination of an equal contribution to all β-pyrrole positions due to σ spin delocalization via the $d_{x^2-y^2}$ unpaired electron (*24*, *58*, *59*) and either equal or unequal contributions to the various β-pyrrole positions due to π spin delocalization via the d_{xz} and d_{yz} unpaired electrons; the mechanism by which the contribution from the d_{xz} and d_{yz} unpaired electrons can become unequal must involve the participation of the protein-provided axial ligand to the heme iron.

It has been shown previously that while low-spin ferrihemes utilize the filled 3e(π) orbitals of the porphyrinate ring for spin delocalization, high-spin ferrihemes utilize the 4e(π*) orbitals for delocalization of π spin density from the metal to the porphyrinate ligand (*24*, *58*, *59*). Because the 4e(π*) orbitals are empty, the direction of spin transfer is from iron to porphyrin in this case, rather than the reverse, as is found for low-spin ferrihemes (*24*, *58*, *59*). This reversal in the direction of spin transfer is reasonable in terms of the high-spin state of these types of ferriheme centers, in that the e(π) symmetry metal orbitals that can engage in this π-back-bonding to the porphyrinate ring, d_{xz} and d_{yz}, are expected to be higher in energy than they would be in the low-spin complexes, and thus are better able to interact with the LUMOs of the porphyrin ring, the 4e(π*) orbitals, rather than the 3e(π) orbitals that are the HOMO-2 filled orbitals of the porphyrin ring (*24*, *58*, *59*).

Since for high-spin Fe(III) the d_{xz} and d_{yz} orbitals each contain an unpaired electron, for model high-spin ferrihemes, where the fifth ligand either has no nodal plane (halides) or has freely spinning ligands (THF or DMSO), there is no preferential delocalization of π spin density to some β-pyrrole positions but not others (*24*), and hence, all equivalent substituents have the same isotropic shift (or similar shifts in cases where the symmetry is lowered, as for protohemin). But the imidazole ring of the proximal histidine of many high-spin ferriheme proteins also has both filled and empty π symmetry orbitals, and could thus interact with one of these two orbitals, but not the other. For low-spin ferrihemes, we usually think of imidazoles as being π donor ligands (*60*). While it is not clear whether this is also the case for the high-spin ferrihemes, if π donation were the mode of interaction between the histidine imidazole ring and the HS Fe(III) center, then we would expect that π donation from

the imidazole p_π HOMO orbital with large amplitude at the nitrogen that binds to iron would produce a partial hole in that imidazole π orbital, meaning that the unpaired electron is largely on the imidazole ring. Hence, the particular d_π unpaired electron that can interact with the imidazole p_π orbital (let us say the one in the d_{yz} orbital, meaning that the imidazole nodal plane is the *xz* plane) would be less available to back-donate to the 4e(π_x*) orbital having its nodal plane in the *xz* plane than would the other d_π unpaired electron (the one in the d_{xz} orbital), which has its nodal plane oriented at 90° to the nodal plane of the histidine imidazole, as shown in Figure 7B. Hence, the interaction of the d_{xz} orbital with its symmetry appropriate 4e(π_y*) orbital would be more important in causing π spin delocalization to the heme substituents.

If the histidine imidazole ligand instead acts as a π acceptor toward the HS Fe(III) center by using its π* LUMO having large amplitude at the bonding nitrogen, then HS Fe(III) would back-bond to this axial histidine π* orbital, again using the d_{yz} metal orbital, thus again making it less able to back-donate to the 4e(π_x*) porphyrin orbital having the *xz* plane as its nodal plane, again leaving the d_{xz} unpaired electron to π back-bond mainly to the 4e(π_y*) orbital oriented at 90° to the nodal plane of the histidine imidazole, as shown in Figure 7B. Hence, in either case, the *yz* plane is predicted to be the nodal plane of the 4e(π*) orbital used for the majority of the spin delocalization onto the heme substituents of the high-spin ferriheme center that has the histidine imidazole ring lying in the *xz* plane, which hence creates an orientation of the nodal plane of the porphyrin ring that determines the order of heme methyl resonances that is 90° rotated from that which would be predicted by the orientation of the histidine imidazole nodal plane shown in Figure 8A (*41*).

The spreads in heme methyl shifts for the high-spin ferriheme proteins, except for elephant met-Mb species A, are relatively similar (within ~20%) to those observed for the low-spin ferriheme protein counterparts (Table 4). This suggests that there is very little residual contribution from the d_π unpaired electron that is involved in delocalization to the histidine imidazole ligand to the shifts of the heme methyls, and thus, only one of the d_π orbitals contributes to spin delocalization within the porphyrin ring; it is also true that the orbital coefficients are somewhat different for the 4e(π*) and 3e(π) orbitals of the porphyrin ring (*61*), which could also contribute to the difference in the spread of the methyl resonances for high- and low-spin ferriheme centers of the same protein. Obviously, the magnitudes of the heme methyl shifts are different in the high-spin and in the low-spin Fe(III) case, so only the order of heme methyl resonances is provided in Figure 7A (*41*). Furthermore, the yellow region representing the approximate position of the diamagnetic envelope of the protein ^{1}H NMR spectrum is appropriate only for the low-spin case; for the high-spin ferriheme proteins, all four heme methyl resonances are always found outside the diamagnetic envelope because of the large σ delocalization contribution from the $d_{x^2-y^2}$ unpaired electron (*24*, *25*, *30*).

In attempting to use this 90° angle shift argument to explain the heme methyl resonance order for cytochrome *c*′ (8 > 1 > 5 > 3), we need to mention three things. First, although the *meso*-H resonances move nearly 100 ppm on going from five- to six-coordinate high-spin ferriheme centers (*24*), the β-pyrrole substituent resonances are affected comparatively little by the coordination number of the iron. Second, having heme methyl resonance shifts ordered 1 > 5 is very unusual among low-spin ferriheme proteins (*38*), but because the substituent effect of the 2,4-thioether groups of *c* cytochromes is clearly much smaller than that of the 2,4-vinyl groups of *b* cytochromes, it is not impossible for the 1 > 5 order to be observed for a *c* cytochrome; furthermore, the substituent effect of the vinyl groups of heme *b* may not be as important for high-spin ferrihemes as it is for low-spin ferrihemes, for we also find the 1 > 5 order for one of the L → V mutants of NP2 (*43*) (Table 4). Third, on the basis of the arguments just presented for high-spin NP2 and its mutants, met-Mb, and HRP, the observed order of the heme methyl resonances (8 > 1 > 5 > 3) for *Rh. palustris* cytochrome *c*′ implies a porphyrin ring nodal plane angle of ~55−65°, which implies a histidine imidazole plane orientation of ~150 ± 10°. Cytochrome *c*′ does not readily bind a sixth ligand (*62*, *63*), so the order of the heme methyl resonances in the low-spin complex has not been determined in that manner. In fact, the orientation of the histidine imidazole plane is ~135° for this cytochrome *c*′ in the solid state (*50*−*56*). This is close to the range suggested by the pattern of high-spin ferriheme methyl resonances presented in Table 4 using the plot of Figure 7A with the 90° adjustment (150 ± 10°) (*41*), but it may suggest some (5−10°) difference between solid state and solution histidine imidazole plane orientations. Hence, again for *c*′ cytochromes, the pattern of heme methyl resonances predicted on the basis of a 90° difference from the angle of the axial ligand plane appears to be observed. It will be interesting to see if other high-spin ferriheme proteins having one histidine ligand bound to the Fe(III) center also have the order of heme methyl resonances predicted by this 90° rotation of the porphyrin nodal plane from that expected for the low-spin Fe(III) proteins (*38*), but on the basis of the systems investigated thus far (met-Mb, HRP, cytochrome *c*′, and NP2 and its mutants), it is likely that this explanation of the patterns of heme methyl resonances in high-spin ferriheme proteins will stand. In fact, using the 90° rotation of the nodal plane, we could consider using the pattern of high-spin Fe(III) methyl peaks as a means of determining the exact angle for the axial histidine imidazole plane, in which case the angle for NP2 is exactly 135°, while those of the distal pocket mutants are slightly larger, as presented in Table 4 and ref *43*.

While a different explanation for the heme methyl shifts of reduced cytochrome *c*′, which contains high-spin Fe(II), has been suggested [one assuming approximately equal and nearly opposing contributions from the dipolar and contact interactions (*64*)], it is clear that this explanation will not work for high-spin Fe(III) proteins because although the two contributions are of opposite sign in this case as well, the size of the dipolar shift is known to be much smaller than that of the contact shift (*58*, *59*). It is also possible that the 90° rotation of the nodal plane that we have found for high-spin Fe(III) heme proteins would work equally well for high-spin Fe(II) heme proteins if the dipolar contribution is considerably smaller in magnitude than the contact contribution. However, the small magnitude of the Fe(II) shifts, and the negative sign of the chemical shift of one of the heme

methyls of ferrocytochrome *c*′ (*64*), certainly both argue that the magnitude of the dipolar contribution is large, and almost equal to that of the contact contribution, as suggested previously.

Summary. We have assigned the heme substituent resonances for two exogenous imidazole ligand complexes of NP2 and have determined the approximate orientation of the nodal plane of the 3e(π) orbital utilized for spin delocalization using the plot of Figure 7A. The angles that have been determined (162 ± 2° for the NP2−NMeIm complex and 150−155° for the NP2−ImH complex) are both larger than that found for the orientation of the imidazole ring of His-57 in the crystal structure of NP2 (130°) (*15*). Thus, the exogenous ligand exerts a larger influence on the orientation of the nodal plane of the heme orbital than does the His-57 imidazole plane. For high-spin NP2, the order of heme methyl resonances found is that predicted for a 90° shift in the orientation of the nodal plane of the heme orbital utilized for spin delocalization (*41*). This 90° shift is explained in terms of a reversal in the direction of spin delocalization (from Por → Fe for the low-spin complexes to Fe → Por for the high-spin complexes) (*24*, *58*, *59*) and is shown schematically in Figure 7B. The exact overlap of the 5Me and 8Me resonances of NP2 indicates a His-57 ligand plane angle of 135° in aqueous solution at pH 7.0. The spread of the heme methyl resonances for high-spin ferriheme proteins is generally on the same order of magnitude as that found for the corresponding low-spin ferriheme protein, which is consistent with an almost complete use of only one d_π metal electron for spin delocalization into one of the two 4e(π*) orbitals; in the low-spin case, only one of the 3e(π) orbitals is involved in π spin delocalization. However, the orbital coefficients for the 4e(π*) and 3e(π) porphyrin orbitals are somewhat different, hence leading to somewhat different spin densities for the two spin states; much larger spreads, and also differences in the average heme methyl shift, may suggest stronger participation of the histidine imidazole, for example, by partial imidazolate formation through hydrogen bonding of the NH group or deprotonation, or other as yet unknown factors. Treating the histidine imidazole as either a π donor or a π acceptor leads to the same prediction of this 90° shift in the nodal plane of the heme orbital utilized for spin delocalization.

SUPPORTING INFORMATION AVAILABLE

Detailed assignment of heme resonances for the NP2−NMeIm complex and 1D and 2D NMR spectra of the NP2−ImH complex and NOESY cross-peak intensities for the NP2−NMeIm complex (Figures S1−S4). This material is available free of charge via the Internet at http://pubs.acs.org.

REFERENCES

1. Walker, F. A., and Montfort, W. R. (2001) The Nitric Oxide-Releasing Heme Proteins from the Saliva of the Blood-Sucking Insect *Rhodnius prolixus*, in *Advances in Inorganic Chemistry* (Mauk, A. G., and Sykes, A. G., Eds.) Vol. 51, Chapter 5, pp 295−358, Academic Press, San Diego.
2. Valenzuela, J. G., Walker, F. A., and Ribeiro, J. M. C. (1995) A Salivary Nitrophorin (NO-Carrying Heme Protein) in the Bedbug, *Cimex lectularius*, *J. Exp. Biol. 198*, 1519−1526.
3. Ribeiro, J. M. C., and Nussenzveig, R. H. (1993) Nitric Oxide Synthase Activity from a Hematophagous Insect Salivary Gland, *FEBS Lett. 330*, 165−168.
4. Nussenzveig, R. H., Bentley, D. L., and Ribeiro, J. M. C. (1995) Nitric-Oxide Loading of the Salivary Nitric-Oxide-Carrying Hemoprotein (Nitrophorin) in the Bloodsucking Bug *Rhodnius prolixus*, *J. Exp. Biol. 198*, 1093−1098.
5. Yuda, M., Hirai, M., Miura, K., Matsumura, H., Ando, K., and Chinzei, Y. (1996) cDNA Cloning, Expression and Characterization of Nitric-Oxide Synthase from the Salivary Glands of the Blood-Sucking Insect *Rhodnius prolixus*, *Eur. J. Biochem. 242*, 807−812.
6. Ribeiro, J. M. C., Hazzard, J. M. H., Nussenzveig, R., Champagne, D., and Walker, F. A. (1993) Reversible Binding of Nitric Oxide by a Salivary Nitrosylheme Protein from the Blood Sucking Insect, *Rhodnius prolixus*, *Science 260*, 539−541.
7. Feltham, R. D., and Enemark, J. H. (1974) Principles of Structure, Bonding, and Reactivity for metal Nitrosyl Complexes, *Coord. Chem. Rev. 13*, 339−406.
8. Ribeiro, J. M. C., and Walker, F. A. (1994) High Affinity Histamine-Binding and Anti-Histaminic Activity of the Salivary NO-Carrying Heme Protein of *Rhodnius prolixus*, *J. Exp. Med. 180*, 2251−2257.
9. Kirchhoff, L. V. (1993) American Trypanosomiasis (Chagas' Disease). A Tropical Disease Now in the United States, *N. Engl. J. Med. 329*, 639−644.
10. Maes, E. M., Walker, F. A., Montfort, W. R., and Czernuszewicz, R. S. (2001) A Resonance Raman Spectroscopic Study of Nitrophorin 1, a Nitric Oxide-Binding Heme Protein from the Saliva of the Blood-Sucking Insect *Rhodnius prolixus*, and its NO and Cyanide Adducts, *J. Am. Chem. Soc. 123*, 11664−11672.
11. Ding, X. D., Weichsel, A., Andersen, J. F., Shokhireva, T. K., Balfour, C., Pierik, A. J., Averill, B. A., Montfort, W. R., and Walker, F. A. (1999) Nitric Oxide Binding to the Ferri- and Ferroheme States of Nitrophorin 1, a Reversible NO-Binding Heme Protein from the Saliva of a Blood-Sucking Insect, *Rhodnius prolixus*, *J. Am. Chem. Soc. 121*, 128−138.
12. Andersen, J. F., Ding, X. D., Balfour, C., Champagne, D. E., Walker, F. A., and Montfort, W. R. (2000) Kinetics and Equilibria in Ligand Binding by Nitrophorins 1−4: Evidence for Stabilization of a NO−Ferriheme Complex through a Ligand-Induced Conformational Trap, *Biochemistry 39*, 10118−10131.
13. Andersen, J. F., Champagne, D. E., Weichsel, A., Ribeiro, J. M. C., Balfour, C. A., Dress, V., and Montfort, W. R. (1997) Nitric Oxide Binding and Crystallization of Recombinant Nitrophorin 1, a Nitric Oxide Transport Protein from the Blood-Sucking Bug *Rhodnius prolixus*, *Biochemistry 36*, 4423−4428.
14. Weichsel, A., Andersen, J. F., Champagne, D. E., Walker, F. A., and Montfort, W. R. (1998) Crystal Structures of a Nitric Oxide Transport Protein from a Blood-Sucking Insect, *Nat. Struct. Biol. 5*, 304−309.
15. Andersen, J. F., and Montfort, W. R. (2000) The Crystal Structure of Nitrophorin 2. A Trifunctional Antihemostatic Protein from the Saliva of *Rhodnius prolixus*, *J. Biol. Chem. 275*, 30496−30503.
16. Andersen, J. F., Weichsel, A., Balfour, C. A., Champagne, D. E., and Montfort, W. R. (1998) The Crystal Structure of Nitrophorin 4 at 1.5 Å Resolution: Transport of Nitric Oxide by a Lipocalin-Based Heme Protein, *Structure 6*, 1315−1327.
17. Weichsel, A., Andersen, J. F., Roberts, S. A., and Montfort, W. R. (2000) Nitric Oxide Binding to Nitrophorin 4 Induces Complete Distal Pocket Burial, *Nat. Struct. Biol. 7*, 551−554.
18. Roberts, S. A., Weichsel, A., Qiu, Y., Shelnutt, J. A., Walker, F. A., and Montfort, W. R. (2001) Ligand-Induced Heme Ruffling and Bent NO Geometry in Ultra-High-Resolution Structures of Nitrophorin 4, *Biochemistry 40*, 11327−11337.
19. Montfort, W. R., Weichsel, A., and Andersen, J. F. (2000) Nitrophorins and Related Antihemostatic Lipocalins from *Rhodnius prolixus* and Other Blood-Sucking Arthropods, *Biochim. Biophys. Acta 1482*, 110−118.
20. Gong, W., Hao, B., Mansy, S. S., Gonzalez, G., Gillies-Gonzalez, M. A., and Chan, M. K. (1998) Structure of a Biological Oxygen Sensor: A New Mechanism for Heme-Driven Signal Transduction, *Proc. Natl. Acad. Sci. U.S.A. 95*, 15177−15182.
21. Hao, B., Isaza, C., Arndt, J., Soltis, M., and Chan, M. K. (2002) Structure-Based Mechanism of O_2 Sensing and Ligand Discrimination by the FixL Heme Domain of *Bradyrhizobium japonicum*, *Biochemistry 41*, 12952−12958.
22. Ribeiro, J. M. C., Schneider, M., and Guimaraes, J. A. (1995) Purification and Characterization of Prolixin S (Nitrophorin 2), the Salifary Anticoagulant of the Blood-Sucking Bug, *Rhodnius prolixus*, *Biochem. J. 308*, 243−249.

23. Zhang, Y., Ribeiro, J. M. C., Guimaraes, J. A., and Walsh, P. N. (1998) Nitrophorin 2: A Novel Mixed-Type Reversible Specific Inhibitor of the Intrinsic Factor-X Activating Complex, *Biochemistry 37*, 10681−10690.
24. Walker, F. A. (2000) Proton NMR and EPR Spectroscopy of Paramagnetic Metalloporphyrins, in *The Porphyrin Handbook* (Kadish, K. M., Smith, K. M., and Guilard, R., Eds.) Vol. 5, Chapter 36, pp 81−183, Academic Press, San Diego.
25. La Mar, G. N., Satterlee, J. D., and De Ropp, J. S. (2000) Nuclear Magnetic Resonance of Hemoproteins, in *The Porphyrin Handbook* (Kadish, K. M., Smith, K. M., and Guilard, R., Eds.) Vol. 5, Chapter 37, pp 185−298, Academic Press, San Diego.
26. Shokhireva, T. Kh., Smith, K. M., Andersen, J. F., Weichsel, A., Balfour, C., Montfort, W. R., and Walker, F. A. (2003) Assignment of Heme Resonances and Determination of Axial Ligand Plane Orientation of the Paramagnetic Complexes of Nitrophorins 1−4 with Imidazole, Histamine and Cyanide by ^{1}H NMR Spectroscopy (manuscript in preparation).
27. Shokhireva, T. Kh., Shokhirev, N. V., and Walker, F. A. (2003) ^{1}H NMR Spectroscopic Studies of the Dynamics of the Axial Ligand Complexes of the Nitrophorins 1−4, Reversible NO-Carrying Heme Proteins from the Saliva of the Blood-Sucking Insect *Rhodnius prolixus* (manuscript in preparation).
28. Bertini, I., Luchinat, C., Macinai, R., Martinuzzi, S., Pierattelli, R., and Viezzoli, R. S. (1998) Isolation and characterization of a cytochrome c_2 from *Rhodopseudomonas palustris*, *Inorg. Chim. Acta 269*, 125−134.
29. Krishnamoorthi, R., La Mar, G. N., Mizukami, H., and Romero, A. (1984) A Proton NMR Investigation of the Influence of Distal Glutamine on Structural and Dynamic Properties of Elephant Metmyoglobin, *J. Biol. Chem. 259*, 265−270.
30. Rajarathanam, K., La Mar, G. N., Chiu, M. L., Sligar, S. G., Singh, J. P., and Smith, K. M. (1991) ^{1}H NMR Hyperfine Shift Pattern as a Probe for Ligation State in High-Spin Ferric Hemoproteins: Water Binding in Metmyoglobin Mutants, *J. Am. Chem. Soc. 113*, 7886−7892.
31. La Mar, G. N., Jackson, J. T., Dugad, L. B., Cusanovich, M. A., and Bartsch, R. G. (1990) Proton NMR Study of the Comparative Electronic/Magnetic Properties and Dynamics of the Acid ⇌ Alkaline Transition in a Series of Ferricytochromes *c*′, *J. Biol. Chem. 265*, 16173−16178.
32. Bertini, I., Gori, G., Luchinat, C., and Vila, A. J. (1993) One- and Two-Dimensional NMR Characterization of Oxidized and Reduced Cytochrome *c*′ from *Rhodocyclus gelatinosus*, *Biochemistry 32*, 776−783.
33. Clark, K., Dugad, L. B., Bartsch, R. G., Cusanovich, M. A., and La Mar, G. N. (1996) An Interpretive Basis of the Proton Nuclear Resonance Hyperfine Shifts for Structure Determination of High-Spin Ferric Hemoproteins. Implications for the Reversible Thermal Unfolding of Ferricytochrome *c*′ from *Rhodopseudomonas palustris*, *J. Am. Chem. Soc. 118*, 4654−4664.
34. De Ropp, J. S., and La Mar, G. N. (1991) 2D NMR Assignment of Hyperfine-Shifted Resonances in Strongly Paramagnetic Metalloproteins: Resting-State Horseradish Peroxidase, *J. Am. Chem. Soc. 113*, 4348−4350.
35. De Ropp, J. S., Mandal, P., Brauer, S. L., and La Mar, G. N. (1997) Solution NMR Study of the Electronic and Molecular Structure of the Heme Cavity in High-Spin, Resting State Horseradish Peroxidase, *J. Am. Chem. Soc. 119*, 4732−4739.
36. Houston, H. L. (1995) The Purification and Physical Characterization of the Reversibly Binding Nitric Oxide Heme Protein of *Rhodnius prolixus*, M.S. Thesis, University of Arizona, Tucson, AZ.
37. King, B. C., Hawkridge, F. M., and Hoffman, B. M. (1992) Electrochemical Studies of Cyanometmyoglobin and Metmyoglobin: Implications for Long-Range Electron Transfer in Proteins, *J. Am. Chem. Soc. 114*, 10603−10608.
38. Shokhirev, N. V., and Walker, F. A. (1998) The Effect of Axial Ligand Plane Orientation on the Contact and Pseudocontact Shifts of Low-Spin Ferriheme Proteins, *J. Biol. Inorg. Chem. 3*, 581−594.
39. Berry, R. E., Ding, X. D., Weichsel, A., Montfort, W. R., and Walker, F. A. (2003) Axial Ligand Complexes of Nitrophorins. Electrochemistry, Binding Constants and Structures of the Imidazole and 4-Iodopyrazole Complexes, *J. Biol. Inorg. Chem.* (submitted for publication).
40. Shokhirev, N. V., and Walker, F. A. (1998) Co/Counter-Rotation of Magnetic Axes and Axial Ligands in Low-Spin Ferriheme Systems, *J. Am. Chem. Soc. 120*, 981−990.
41. *Heme Methyl Shift Patterns*, http://www.chem.arizona.edu/~shokhirn/nikolai/programs/prgsciedu.html or http://www.chem.arizona.edu/~shokhirn/nikolai/programs/prog/ShiftPatterns.zip.
42. Unpublished work from this laboratory.
43. Shokhireva, T. Kh., Berry, R. E., Uno, E., Balfour, C. A., Zhang, H., and Walker, F. A. (2003) Electrochemical and NMR Spectroscopic Investigations of the Single and Double Distal Pocket Mutants L122,132V of Nitrophorin 2: The Effect of Altering Cavity Size on Stability, Structure and Dynamics of Axial Ligand Complexes, *Proc. Natl. Acad. Sci. U.S.A.* (submitted for publication).
44. Rae, T. D., and Goff, H. M. (1996) Lactoperoxidase Heme Structure Characterized by Paramagnetic Proton NMR Spectroscopy, *J. Am. Chem. Soc. 118*, 2103−2104.
45. Kachalova, G. S., Popov, A. N., and Bartunik, H. D. (1999) A Steric Mechanism for Inhibition of CO Binding to Heme Proteins, *Science 284*, 473−476.
46. Liong, E. C., Dou, Y., Scott, E. E., Olson, J. S., and Phillips, G. N. (2001) Waterproofing the Heme Pocket. Role of Proximal Amino Acid Side Chains in Preventing Hemin Loss from Myoglobins, *J. Biol. Chem. 276*, 9093−9100.
47. Urayama, P., Phillips, G. N., Jr., and Gruner, S. M. (2002) Probing Substrates in Sperm Whale Myoglobin Using High-Pressure Crystallography, *Structure 10*, 51−60.
48. Morita, Y., Mikami, B., Yamashita, H., Lee, J. Y., Aibara, S., Sato, M., Katsube, Y., and Tanaka, N. (1991) Primary and Crystal Structures of Horseradish Peroxidase Isozyme E5, in *Biochemical, Molecular and Physiological Aspects of Plant Peroxidases* (Lobarzewski, J., Greppin, H., Penel, C., and Gaspar, T., Eds) pp 81−88, University of Geneva, Geneva, Switzerland.
49. Poulos, T L., Edwards, S. L., Warishi, H., and Gold, M. H. (1993) Crystallographic Refinement of Lignin Peroxidase at 2.0 Å Resolution, *J. Biol. Chem. 268*, 4429−4440.
50. Finzel, B. C., Weber, P. C., Hardman, K. D., and Salemme, F. R. (1985) Structure of Ferricytochrome *c*′ from *Rhodospirillum molischianum* at 1.67 Å Resolution, *J. Mol. Biol. 186*, 627−643.
51. Yasui, M., Harada, S., Kai, Y., Kasai, N., Kusonoki, M., and Matsuura, Y. (1992) Three-Dimensional Structure of Ferricytochrome *c*′ from *Rhodospirillum rubrum* at 2.8 Å Resolution, *J. Biochem. 111*, 317−324.
52. Ren, Z., Meyer, T., and McRee, D. E. (1993) Atomic Structure of a Cytochrome *c*′ with an Unusual Ligand-controlled Dimer Dissociation at 1.8 Å Resolution, *J. Mol. Biol. 234*, 433−445.
53. Archer, M., Banci, L., Dikaya, E., and Romão, M. J. (1997) Crystal Structure of Cytochrome *c*′ from *Rhodocyclus gelatinosus* and Comparison with Other Cytochromes *c*′, *J. Biol. Inorg. Chem. 2*, 611−622.
54. Tahirov, T. H., Misaki, S., Meyer, T. E., Cusanovich, M. A., Higuchi, Y., and Yasuoka, N. (1996) High-resolution Crystal Structures of Two Polymorphs of Cytochrome *c*′ from the Purple Phototrophic Bacterium *Rhodobacter capsulatus*, *J. Mol. Biol. 259*, 467−479.
55. Dobbs, A. J., Anderson, B. F., Faber, H. R., and Baker, E. N. (1996) Three-Dimensional Structure of Cytochrome *c*′ from Two *Alcaligenes* Species and the Implications for Four-Helix Bundle Structures, *Acta Crystallogr. D52*, 356−368.
56. Shibata, N., Iba, S., Misaki, S., Meyer, T. E., Bartsch, R. G., Cusanovich, M. A., Morimoto, Y., Higuchi, Y., and Yasuoka, N. (1998) Basis for Monomer Stabilization in *Rhodopseudomonas palustris* Cytochrome *c*′ Derived from the Crystal Structure, *J. Mol. Biol. 284*, 751−760.
57. Watson, H. C., and Kendrew, J. C. (1969) The Stereochemistry of the Protein Myoglobin, *Prog. Stereochem. 4*, 299.
58. Walker, F. A., and La Mar, G. N. (1973) Nuclear Magnetic Resonance Studies of Ferric Porphyrins, *Ann. N.Y. Acad. Sci. 206*, 328−348.
59. La Mar, G. N., and Walker, F. A. (1979) NMR Studies of Paramagnetic Metalloporphyrins, in *The Porphyrins* (Dolphin, D., Ed.) Vol. IV, pp 61−157, Academic Press, New York.
60. Safo, M. K., Gupta, G. P., Watson, C. T., Simonis, U., Walker, F. A., and Scheidt, W. R. (1992) Models of the Cytochromes *b*. Low-Spin Bis-Ligated (Porphinato)Iron(III) Complexes with 'Unusual' Molecular Structures, NMR, EPR, and Mössbauer Spectra, *J. Am. Chem. Soc. 114*, 7066−7075.
61. Longuet-Higgins, H. C., Rector, C. W., and Platt, J. R. (1950) Molecular Orbital Calculations on Porphine and Tetrahydroporphine, *J. Chem. Phys. 18*, 1174−1181.

62. Kassner, R. J., Kykta, M. G., and Cusanovich, M. A. (1985) Binding of Cyanide to Cytochrome *c′* from *Chromatium vinosum*, *Biochim. Biophys. Acta 831*, 155−158.
63. Motie, M., Kassner, R. J., Meyer, T. E., and Cusanovich, M. A. (1990) Kinetics of Cyanide Binding to *Chromatium vinosum* Ferricytochrome *c′*, *Biochemistry 29*, 1932−1936.
64. Bertini, I., Dikiy, A., Luchinat, C., Macinai, R., and Viezzoli, M. S. (1998) ^{1}H NMR Study of the Reduced Cytochrome *c′* from *Rhodopseudomonas palustris* Containing a High-Spin Iron(II) Heme Moiety, *Inorg. Chem. 37*, 4814−4821.
65. Budd, D. L., La Mar, G. N., Langry, K. C., Smith, K. M., and Nayyir, R. (1979) Proton NMR Study of High-Spin Ferric Natural Porphyrin Derivatives as Models of Methemoglobins, *J. Am. Chem. Soc. 101*, 6091−6096.
66. La Mar, G. N., Viscio, D. B., Smith, K. M., Caughey, W. S., and Smith, M. L. (1978) NMR Studies of Low-Spin Ferric Complexes of Natural Porphyrin Derivatives. 1. Effect of Peripheral Substituents on the Electronic Asymmetry in Bis-cyano Complexes, *J. Am. Chem. Soc. 100*, 8085−8092.
67. La Mar, G. N., Emerson, S. D., Lecomte, J. T. J., Pande, U., Smith, K. M., Craig, G. W., and Kehres, L. A. (1986) Influence of Propionate Side Chains on the Equilibrium Heme Orientation in Sperm Whale Myoglobin. Heme Resonance Assignments and Structure Determination by Nuclear Overhauser Effect Measurements, *J. Am. Chem. Soc. 108*, 5568−5573.
68. Vyas, K., Rajarthanam, K., Yu, L. P., Emerson, S. D., and La Mar, G. N. (1993) ^{1}H NMR Investigation of the Heme Cavity of Elephant (E7 Gln) Met-cyano-myoglobin. Evidence for a B-Helix Phenylalanine Interaction with Bound Ligand, *J. Biol. Chem. 268*, 14826−14835.
69. Chen, Z., de Ropp, J. S., Hernandez, G., and La Mar, G. N. (1994) 2D NMR Approaches to Characterizing the Molecular Structure and Dynamic Stability of the Active Site for Cyanide-Inhibited Horseradish Peroxidase, *J. Am. Chem. Soc. 116*, 8772−8783.

BI026765W